JACS
JOURNAL OF THE AMERICAN CHEMICAL SOCIETY
pubs.acs.org/JACS
Article

A Photorobust Mo(0) Complex Mimicking $[Os(2,2'\text{-bipyridine})_3]^{2+}$ and Its Application in Red-to-Blue Upconversion

Jakob B. Bilger, Christoph Kerzig, Christopher B. Larsen, and Oliver S. Wenger*

Cite This: J. Am. Chem. Soc. 2021, 143, 1651−1663
Read Online
ACCESS | Metrics & More | Article Recommendations | Supporting Information

ABSTRACT: Osmium(II) polypyridines are a well-known class of complexes with luminescent metal-to-ligand charge-transfer (MLCT) excited states that are currently experiencing a revival due to their application potential in organic photoredox catalysis, triplet−triplet annihilation upconversion, and phototherapy. At the same time, there is increased interest in the development of photoactive complexes made from Earth-abundant rather than precious metals. Against this background, we present a homoleptic Mo(0) complex with a new diisocyanide ligand exhibiting different bite angles and a greater extent of π-conjugation than previously reported related chelates. This new design leads to deep red emission, which is unprecedented for homoleptic arylisocyanide complexes of group 6 metals. With a ^{3}MLCT lifetime of 56 ns, an emission band maximum at 720 nm, and a photoluminescence quantum yield of 1.5% in deaerated toluene at room temperature, the photophysical properties are reminiscent of the prototypical $[Os(2,2'\text{-bipyridine})_3]^{2+}$ complex. Under 635 nm irradiation with a cw-laser, the new Mo(0) complex sensitizes triplet−triplet annihilation upconversion of 9,10-diphenylanthracene (DPA), resulting in delayed blue fluorescence with an anti-Stokes shift of 0.93 eV. The photorobustness of the Mo(0) complex and the upconversion quantum yield are high enough to generate a flux of upconverted light that can serve as a sufficiently potent irradiation source for a blue-light-driven photoisomerization reaction. These findings are relevant in the greater contexts of designing new luminophores and photosensitizers for use in red-light-driven photocatalysis, photochemical upconversion, light-harvesting, and phototherapy.

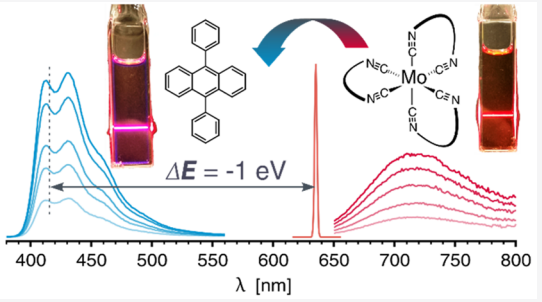

INTRODUCTION

The development of new types of photoactive complexes from Earth-abundant metals and the use of low-energy light to drive thermodynamically challenging photoreactions have become two important interest areas at the interface of coordination chemistry, spectroscopy, solar energy conversion, and synthetic organic photochemistry. Our study addresses both of these interest areas by disclosing a new design concept for Mo(0) isocyanide complexes allowing the establishment of deep red emission from a metal-to-ligand charge transfer (MLCT) excited state, and its exploitation in triplet−triplet annihilation upconversion to generate blue output from red input light.

Polypyridine complexes of precious d^6 metals such as Ru(II), Os(II), and Ir(III) have long played a dominant role as luminophores and photosensitizers in inorganic photophysics and photochemistry,[1] and they continue to be essential for organic photoredox catalysis[2,3] and applications in organic light-emitting diodes (OLEDs),[4] light harvesting, solar energy conversion,[5−8] and phototherapy.[9,10] Traditionally, there has been much focus on Fe(II) and Cu(I) as Earth-abundant alternatives,[11−15] and some remarkable advances have been made with these metals lately.[16−26] In parallel, a broader spectrum of base metals and oxidation states has come into focus recently,[27] leading to new types of complexes with photoactive ligand-to-metal charge transfer (LMCT),[28−31] ligand-centered (LC),[32,33] or metal-centered (MC) excited states.[34−40] Among MLCT luminophores, arylisocyanide complexes of zerovalent group 6 metals represent a promising class of compounds. Building on a few studies from the 1970s[41,42] and newer work on emissive W(0) complexes with monodentate arylisocyanides,[43−45] we discovered that chelating diisocyanide ligands provide access to Cr(0) and Mo(0) complexes (Figure 1A) as Earth-abundant analogues of the $[Ru(bpy)_3]^{2+}$ (bpy = 2,2′-bipyridine) lead compound.[46,47]

Our previous reports of luminescent Mo(0) and Cr(0) complexes all employed chelating diisocyanide ligands based on a *m*-terphenyl backbone. Of particular note, $[Mo(L^2)_3]$ exhibits strong MLCT absorptions out to 550 nm, and bright ^{3}MLCT luminescence at ∼600 nm, substantially improved with respect to $[Mo(L^1)_3]$—which was assigned to the sterically bulky *tert*-butyl groups protecting the metal from the chemical environment.[48]

Received: December 9, 2020
Published: January 12, 2021

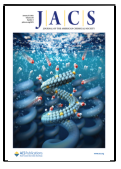

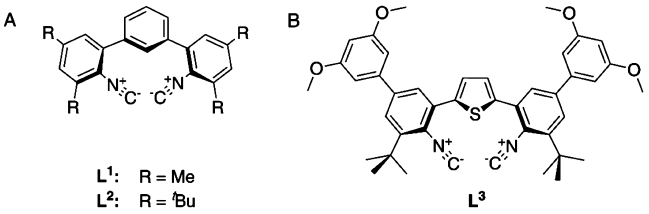

Figure 1. Molecular structures of ligands previously used for Cr(0) and Mo(0) complexes (A)[46−48] and the new ligand (B) yielding the $[Mo(L^3)_3]$ complex reported herein.

With the specific goal of targeting deep red luminescent Mo(0) complexes, we made two significant changes to the ligand design (Figure 1B): (1) replacing the central 6-membered phenylene ring with a 5-membered thiophene ring; (2) replacing the *tert*-butyl groups situated *para* to the isocyanide groups with aryl substituents. These ligand modifications seek to minimize steric restrictions associated with the central ligand ring, thereby facilitating access to ligand conformations with improved bite-angles, and extending the effective ligand π-conjugation to shift MLCT absorption and emission to the red.[49] As a result, we obtained the homoleptic complex, $[Mo(L^3)_3]$, with photophysical properties reminiscent of those of $[Os(bpy)_3]^{2+}$, i.e., deep red ^{3}MLCT luminescence with an excited-state lifetime on the order of 50−90 ns in deaerated solution at room temperature and an unusually high photorobustness. This discovery is relevant in the context of using red excitation light for photochemical reactions, light-harvesting,[50] imaging, or phototherapeutic purposes.[51] Red light is less damaging than UV or blue irradiation,[52] can lead to more selective excitation of photocatalysts in complex reaction mixtures,[53] and can have a deeper penetration depth into reaction media.[54−56] Recently, these aspects and the idea of using low-energy input light to drive photoreactions that would normally require UV or blue irradiation have gained increasing attention in photoredox catalysis.[55,57−68] The sequential absorption of two low-energy photons per catalytic turnover can help fulfill the thermodynamic requirements of a challenging reaction,[69] but this approach relies on efficient red-light absorbers that are sufficiently robust under high irradiation densities. Moreover, intersystem crossing leading to population of the photosensitizer's lowest-lying triplet excited state must be rapid, and one usually faces the challenge that undesired nonradiative relaxation processes become increasingly important the lower the triplet energy gets.[70] So far, mostly certain carefully designed osmium,[71−74] palladium,[66,75−79] and platinum[80−82] complexes fulfill the necessary requirements for red-light absorbing triplet sensitizers, whereas base metal complexes—with the exception of some Cu(I) and Zn(II) compounds[83−85]—have remained underexplored in this context.[86]

$[Mo(L^3)_3]$ satisfies all the necessary conditions for sensitized red-to-blue light upconversion with 9,10-diphenylanthracene (DPA) as the triplet annihilator. $[Mo(L^3)_3]$ tolerates high excitation densities of red light over several hours, enabling the generation of a strong blue-photon flux over extended periods. To illustrate this, a glass tube in which the photochemical upconversion occurs served as the only irradiation source for a separate, blue-light initiated photoreaction.

Our work suggests that a much wider scope of transition metal compounds than what was long considered relevant could be useful as red-light (MLCT) emitters and triplet sensitizers, complementing recent insights gained in the area of metal-free dyes and photosensitizers.[87−95]

Scheme 1. Synthesis of the Ligand L^3 and the Homoleptic $[Mo(L^3)_3]$ Complex[a]

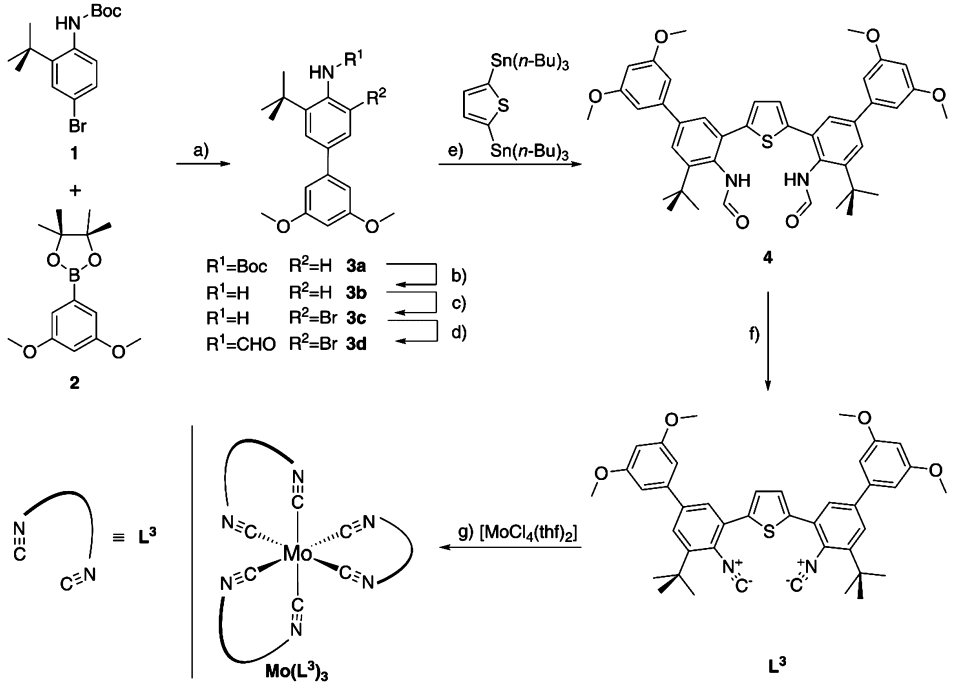

[a]Reagents and conditions: (a) $Pd(PPh_3)_4$, K_2CO_3, dioxane/H_2O, microwave, 90 °C, 97%; (b) TFA, CH_2Cl_2, 0 °C to rt, 94%; (c) NBu_4Br_3, THF, 0 °C, 85%; (d) acetic anhydride, HCOOH, 0 °C to rt, 80%; (e) $PdCl_2$(dppf), xylene, 139 °C, 57%; (f) $POCl_3$, *N*,*N*-diisopropylamine, CH_2Cl_2, 0 °C to rt, 70%; (g) Na/Hg, THF, rt, 23%.

https://dx.doi.org/10.1021/jacs.0c12805
J. Am. Chem. Soc. 2021, 143, 1651−1663

RESULTS AND DISCUSSION

Synthesis and Infrared Spectroscopy. The synthesis of ligand L^3 started with the preparation of compounds **1** and **2** from commercially available precursors (Scheme 1). Specifically, 2-*tert*-butylaniline was brominated using NBu_4Br_3[96] and its amino group subsequently Boc-protected to yield **1**.[97] 1-Bromo-3,5-dimethoxybenzene was Miyaura coupled with bis(pinacolato)diboron to afford **2**. Suzuki coupling of **1** and **2** afforded compound **3a**, which was deprotected using CF_3COOH to yield the aniline **3b**. Bromination of **3b** with NBu_4Br_3 occurred selectively in the *ortho*-position relative to the amino group, resulting in **3c**. Protection of the aniline with formamide (to afford **3d**) was necessary before efficient Stille coupling with commercially available 2,5-bis(tri-*n*-butylstannyl)thiophene was possible. Dehydration of the coupling product **4** gave the final ligand L^3 in 18% overall yield based on the commercially available 2-*tert*-butylaniline precursor. The $[Mo(L^3)_3]$ complex was prepared by reacting 3 equiv of L^3 with $MoCl_4(thf)_2$[98] using Na/Hg as reductant.[43,46] As a powder, the $[Mo(L^3)_3]$ complex can be handled under an ambient atmosphere without noticeable degradation. In dilute solutions, it is sensitive to dissolved oxygen (see SI page S6 for details).

The C≡N stretching frequency (υ_{CN}) of isocyanides is usually very susceptible to metal coordination,[99−101] and this is also the case here. In the IR spectrum of the free ligand, L^3, υ_{CN} is observed at 2112 cm^{-1}, whereas in $[Mo(L^3)_3]$ it is shifted to 1930 cm^{-1} as a result of π-backbonding (Figure S8).[102] Furthermore, the respective IR absorption band is substantially broader in the complex when compared to the free ligand, possibly due to geometric isocyanide distortions as a consequence of strong π-back-donation from the electron-rich Mo(0) center. Due to the change in ligand design incorporating now a central thiophene instead of a phenylene unit between arylisocyanide moieties (Figure 1), we anticipated a significant change in metal coordination. Unfortunately, we were unable to obtain single crystals of $[Mo(L^3)_3]$ to test this hypothesis by X-ray diffraction. However, π-backbonding is significantly stronger in $[Mo(L^3)_3]$ than in $[Mo(L^2)_3]$ based on the observable shift of υ_{CN} between free ligand and metal complex, suggesting that L^3 can adopt conformations leading to better metal−ligand orbital overlap and more ideal octahedral coordination of Mo(0) than L^2. Specifically, the free ligands L^3 and L^2 exhibit an identical C≡N stretch frequency of 2112 cm^{-1},[48] indicating that electronic substituent effects have negligible influence on υ_{CN}, but upon coordination to Mo(0), υ_{CN} decreases by 182 cm^{-1} in the case of $[Mo(L^3)_3]$ but only by 161 cm^{-1} in $[Mo(L^2)_3]$. The comparison between L^3 and L^2 is meaningful, because these ligands both feature the same bulky *tert*-butyl substituents in *ortho*-position to the isocyanide group (Figure 1).

Electrochemistry. The cyclic voltammogram of the $[Mo(L^3)_3]$ complex in deaerated THF containing 0.1 M $TBAPF_6$ shows an oxidation wave at 0.1 V vs SCE (Figure 2A), which is attributable to the Mo(0/I) redox couple. The linear relationship between peak current and potential scan rate (Figure 2B) indicates full reversibility of this metal-centered redox process. In the previously investigated $[Mo(L^2)_3]$ complex the Mo(0/I) potential is approximately 0.2 V less positive (−0.08 V vs SCE),[48] suggesting that the largely metal-centered ("t_{2g}"-like) HOMO of $[Mo(L^3)_3]$ is stabilized by ca.

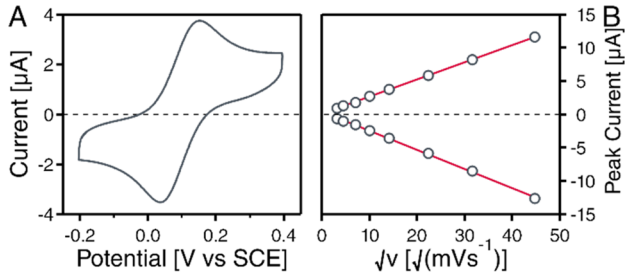

Figure 2. (A) Cyclic voltammogram of the $[Mo(L^3)_3]$ Mo(0/I) redox couple in deaerated THF containing 0.1 M $TBAPF_6$ at 20 °C, recorded with a scan rate of 200 mV/s. (B) Randles−Sevcik plot for the Mo(0/I) redox couple from (A).

0.2 eV relative to that of $[Mo(L^2)_3]$. In the range between 0 and −2.0 V vs SCE, no redox waves are detectable (Figure S9), and thus the reduction potentials of the attached L^3 ligands cannot be directly determined. Based on an energy of the emissive MLCT excited state (E_{MLCT}) of 1.94 eV (see below), we estimate a potential of −1.84 V vs SCE for the Mo(0/I) redox couple in the emissive MLCT excited state (Mo*(0/I)) (Figure S10). Thus, $[Mo(L^3)_3]$ is expected to be a strong photoreductant, although this aspect is not the focus of the present study.

Optical Spectroscopy. $[Mo(L^3)_3]$ exhibits similar UV−vis absorption bands as $[Mo(L^2)_3]$,[48] but all of them are shifted by 3000−8000 cm^{-1} to lower energies (solid black traces in Figure 3). In the UV spectral region, the ligand-centered $\pi-\pi^*$

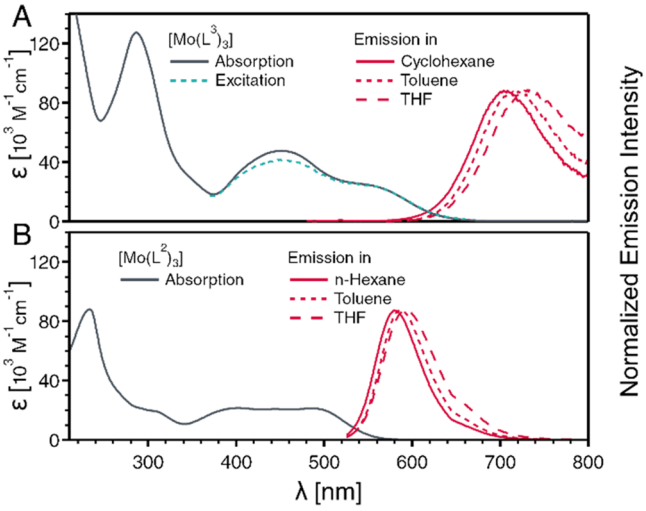

Figure 3. UV−vis absorption spectra of (A) $[Mo(L^3)_3]$ in cyclohexane and (B) $[Mo(L^2)_3]$ in *n*-hexane at 20 °C (solid black traces). Luminescence spectra of (A) $[Mo(L^3)_3]$ and (B) $[Mo(L^2)_3]$ in different deaerated solvents (red traces, see inset) at 20 °C. Excitation occurred at 465 nm for $[Mo(L^3)_3]$ and at 500 nm for $[Mo(L^2)_3]$. The $[Mo(L^2)_3]$ data is from ref 48. The dashed green trace in (A) is the (arbitrarily scaled) excitation spectrum obtained by monitoring the $[Mo(L^3)_3]$ emission in deaerated toluene at 705 nm.

absorption band shifts from 232 nm for the complex with the *m*-terphenyl based ligand (L^2) to 285 nm for the complex with the new 2,5-diphenylthiophene based ligand (L^3), indicating a greater extent of π-conjugation in the latter. In the visible region, the band maximum of the lowest MLCT absorption shifts from 480 nm for $[Mo(L^2)_3]$ to 550 nm in $[Mo(L^3)_3]$. The new ligand design furthermore entails a factor-of-2

https://dx.doi.org/10.1021/jacs.0c12805
J. Am. Chem. Soc. 2021, 143, 1651−1663

Table 1. Photophysical Parameters of Two Mo(0) Complexes and $[M(bpy)_3]^{2+}$ Reference Complexes (M = Os, Ru)[a]

complex	λ_{em}/nm	τ/ns	ϕ	k_r/s^{-1}	k_{nr}/s^{-1}
$[Mo(L^3)_3]$[b]	720	56	0.015	2.6×10^5	1.8×10^7
$[Os(bpy)_3]^{2+}$[c]	723	60	0.00462	7.71×10^4	1.66×10^7
$[Mo(L^2)_3]$[d]	587	1293[e]	0.203		
$[Ru(bpy)_3]^{2+}$[c]	620	855	0.062	7.25×10^4	1.1×10^6

[a]See text for definitions of the individual parameters. [b]In deaerated toluene at 20 °C; this work. [c]In deoxygenated acetonitrile at 23 °C.[105−107] [d]In deaerated toluene at 20 °C; from ref 48. [e]Weighted average value for two conformers with different lifetimes (τ_1 = 1110 ns (85%), τ_2 = 2330 ns (15%)).[48] The calculation of radiative (k_r) and nonradiative decay rate constants (k_{nr}) is not meaningful in this case, because the excited-state decay is biexponential.

increase of the molar extinction coefficients of the visible absorptions. The lowest electronic transitions are likely to have mixed MLCT and $\pi-\pi^*$ (C≡N−C) character based on prior computational studies of W(0) arylisocyanides,[103] enhancing their extinction coefficients. In the $[Mo(L^3)_3]$ complex, the lowest absorption band tails to nearly 680 nm. At 635 nm the extinction coefficient ε_{635} is still 3340 M^{-1} cm^{-1}, which makes efficient photoexcitation with red light possible. The $[Os(bpy)_3]^{2+}$ complex, which has been widely used for red-to-blue upconversion, has a similar molar extinction coefficient at that wavelength ($\varepsilon_{635\ nm} \approx 4000\ M^{-1}\ cm^{-1}$),[104] though in this case the relevant electronic transition is a formally spin-forbidden singlet−triplet absorption. In $[Mo(L^3)_3]$, excitation at 635 nm occurs into a spin-allowed absorption band, yet the energy loss associated with intersystem crossing (ISC) to the lowest triplet state remains favorably small in this case (see below).

$[Mo(L^3)_3]$ shows red luminescence at room temperature, with band maxima (λ_{em}) at 705, 720, and 730 nm in cyclohexane, toluene, and THF, respectively (red traces in Figure 3A). Compared to $[Mo(L^2)_3]$ under comparable conditions,[48] this corresponds to a red shift of ca. 3000 cm^{-1}, in line with the MLCT absorption band shifts described above. The observable emission solvatochromism is as expected for MLCT states, in which the dipole moment is larger than in the electronic ground state. The excitation spectrum of the $[Mo(L^3)_3]$ luminescence detected at 705 nm (dashed green trace in Figure 3A) closely follows the UV−vis absorption spectrum, indicating that higher lying excited states ultimately lead to population of the lowest (emissive) excited state. From an emission spectrum recorded in 2-methyl-THF at 77 K, an MLCT energy (E_{MLCT}) of 1.94 eV can be estimated (Figure S12).

The photoluminescence quantum yield (ϕ) of $[Mo(L^3)_3]$ in deaerated toluene at 20 °C is 0.015 (Table 1), approximately 13 times lower than that for $[Mo(L^2)_3]$ under identical conditions (ϕ = 0.203).[48] Given the markedly lower MLCT energy in $[Mo(L^3)_3]$, this is unsurprising in light of the energy gap law.[70] In prior studies of Os(II)-based emitters, a decrease in MLCT energy by 3000 cm^{-1} caused an increase of the rate constant for nonradiative MLCT deactivation by a factor of ca. 30, lowering ϕ by roughly the same factor.[105] For reference, the emission quantum yield for $[Os(bpy)_3]^{2+}$ is 0.00462 in deoxygenated CH_3CN at 23 °C,[105] roughly 3 times lower than that for $[Mo(L^3)_3]$ (Table 1).

The transient absorption spectrum recorded after pulsed excitation of $[Mo(L^3)_3]$ at 532 nm (Figure 4A) exhibits a bleach in the region of the MLCT absorption bands with (negative) peaks coinciding with those of the ground-state absorption spectrum (475 and 560 nm in toluene). Also observable is a negative signal around 720 nm due to emission, and an excited-state absorption feature near 375 nm, which is

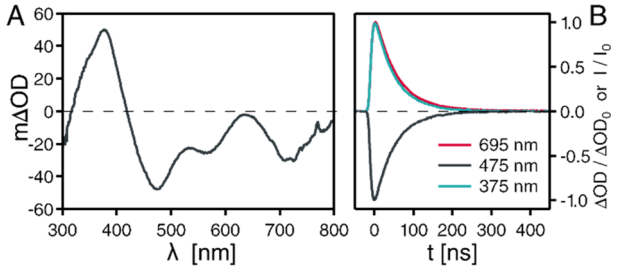

Figure 4. (A) Transient absorption spectrum of 20 μM $[Mo(L^3)_3]$ in deaerated toluene at 20 °C, recorded with a delay time of 20 ns following excitation at 532 nm with pulses of ca. 10 ns duration. The signal was time-integrated over 200 ns. (B) Temporal evolution of the different signals from (A) as indicated in the inset.

attributed to the one-electron reduced ligand of the MLCT state.[48] All of these excited-state absorption features, MLCT bleaches, and emission signals exhibit identical (single-exponential) decay behavior (Figure 4B), yielding an MLCT lifetime (τ) of 56 ns in deaerated toluene at 20 °C. This relatively long lifetime is in line with the expected triplet character of the excited state. The single-exponential ^{3}MLCT kinetics of $[Mo(L^3)_3]$ are in contrast to the biexponential decays of the previously studied $[Mo(L^2)_3]$,[48] which we tentatively attribute to greater conformational flexibility of the thiophene ring of L^3 compared to the central benzene unit of L^2. Based on τ = 56 ns and ϕ = 0.015, the rate constants for radiative (k_r) and nonradiative ^{3}MLCT deactivation (k_{nr}) in deaerated toluene at room temperature are 2.6×10^5 s^{-1} and 1.8×10^7 s^{-1}, respectively (Table 1).

In addition to nonradiative relaxation directly from the excited to the ground state as mentioned above, Ru(II) polypyridine complexes typically exhibit thermally activated nonradiative relaxation pathways involving the population of MC states. While this aspect has received significant attention in Ru(II) polypyridine complexes,[108,109] it has been hitherto neglected in most investigations of group 6 metal isocyanide complexes. The temperature-dependent luminescence lifetime data in Figure 5 allow us to address this issue for $[Mo(L^3)_3]$. Between 10 and 50 °C, the ^{3}MLCT lifetime (τ) of $[Mo(L^3)_3]$ in deaerated toluene decreases by approximately a factor of 2, as observed in Figure 5B ($k_{obs} = \tau^{-1}$). It is well-established that thermally activated nonradiative deactivation through low-lying MC states is best described using a model in which the ^{3}MLCT and ^{3}MC states are thermally equilibrated.[110] The k_{obs} values were therefore fitted using eq 1 (Figure 5B), which is derived from a simple two-state thermally equilibrated model as depicted in Figure 5C,[110,111] and adequately models the observed temperature-dependence of k_{obs}.

https://dx.doi.org/10.1021/jacs.0c12805
J. Am. Chem. Soc. 2021, 143, 1651−1663

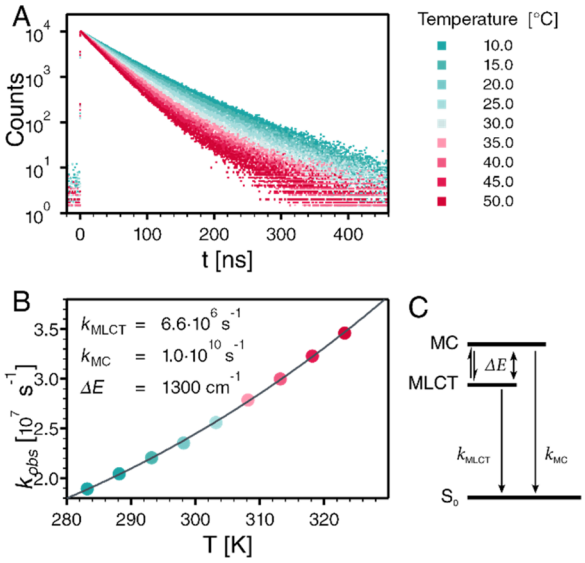

Figure 5. (A) ^{3}MLCT luminescence decays of $[Mo(L^3)_3]$ in deaerated toluene at different temperatures. In this TCSPC experiment, excitation occurred at 475 nm, detection was at 710 nm. (B) Decay rate constants ($k_{obs} = \tau^{-1}$) extracted from the data in (A). The solid gray line is a fit with eq 1 to the experimental data, yielding the parameters given in the inset. (C) Three-state model for ^{3}MLCT excited state decay including thermal population of a nearby MC state; k_{MLCT} is the rate constant for MLCT decay directly to the ground state (encompassing both radiative and nonradiative contributions), and k_{MC} is the rate constant for nonradiative MC state decay to the ground state.

$$k_{obs} = [k_{MLCT} + k_{MC} \times \exp(-\Delta E/k_B \times T)] / [1 + \exp(-\Delta E/k_B \times T)] \quad (1)$$

In this simplistic but common picture, k_{MLCT} is the total (radiative plus nonradiative) ^{3}MLCT excited state decay rate constant for *direct* relaxation to the ground state, k_{MC} is the rate constant for nonradiative relaxation from the thermally populated MC state, ΔE is the energy difference between the MC and ^{3}MLCT state, and k_B is Boltzmann's constant. The best (unconstrained) fit is obtained with $k_{MLCT} = 6.6 \times 10^6$ s^{-1}, $k_{MC} = 1.0 \times 10^{10}$ s^{-1}, and $\Delta E = 1300$ cm^{-1} (solid gray line in Figure 5B). An underlying assumption here is that the observed temperature dependence is caused by varying relative populations of only two excited states (one ^{3}MLCT and one MC state), whereas the k_{MLCT} and k_{MC} parameters themselves are temperature-independent within the investigated range. When further assuming identical degeneracies for the ^{3}MLCT and MC states, the Boltzmann population of the MC state at 298 K is approximately 0.2% of the total excited-state population. The rate for nonradiative depopulation through the MC channel then becomes $0.002 \times k_{MC} = 2 \times 10^7$ s^{-1}, which is on the same order of magnitude as the experimentally determined k_{nr} value (Table 1). This crude approximation therefore suggests that nonradiative ^{3}MLCT relaxation via the MC channel is a major decay path for $[Mo(L^3)_3]$. For comparison, $[Ru(bpy)_3]^{2+}$ and many of its closely related derivatives have ΔE values on the order of 3500 cm^{-1} (0.43 eV),[111,112] and consequently the MC state plays a smaller role for ^{3}MLCT depopulation in these complexes than in $[Mo(L^3)_3]$.

Photostability. Although the photophysical properties of $[Mo(L^3)_3]$ resemble those of $[Os(bpy)_3]^{2+}$, it is meaningful to use $[Ru(bpy)_3]^{2+}$ as a reference point for certain performance factors. On the one hand, this is because Mo(0) and Ru(II) are both isoelectronic second-row transition metals, and on the other hand $[Ru(bpy)_3]^{2+}$ has been an important benchmark compound in many previous investigations.[113] Comparative photostability studies were therefore performed with $[Mo(L^3)_3]$ and $[Ru(bpy)_3]^{2+}$, using solutions with essentially identical absorbance at the excitation wavelength, and photoluminescence was monitored as a function of irradiation time (Figure 6). Mainly for reasons of solubility, but also

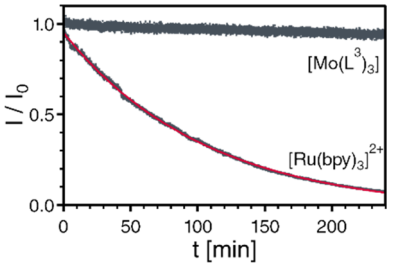

Figure 6. Relative photostability studies. Lower gray trace: Normalized luminescence intensity of 96 μM $[Ru(bpy)_3]^{2+}$ at 620 nm in deaerated acetonitrile under continuous irradiation with a 500 mW laser at 532 nm. Upper gray trace: Normalized luminescence intensity of 3 μM $[Mo(L^3)_3]$ at 710 nm in deaerated toluene under continuous irradiation with a 500 mW laser at 532 nm. The complex concentrations were adjusted such that both samples had essentially identical absorbance (OD approximately 0.08) at the excitation wavelength (see SI page S30 for details). The red trace is an exponential fit to the gray experimental data.

because it is the preferred solvent for the upconversion studies presented below, toluene was used for $[Mo(L^3)_3]$, whereas the reference compound was dissolved in acetonitrile, the most typical solvent for $[Ru(bpy)_3](PF_6)_2$. The excitation source was a cw-laser with 500 mW output at 532 nm, which irradiated the two solutions in common 1 cm quartz cuvettes inside a fluorimeter. The time traces in Figure 6 represent the luminescence intensities at (or near) the respective emission maxima (710 nm for $[Mo(L^3)_3]$, 620 nm for $[Ru(bpy)_3]^{2+}$), normalized to the initial intensity at the start of the irradiation period. Over the span of 4 h, the emission intensity of $[Ru(bpy)_3]^{2+}$ decreases to less than 10% of its initial value, closely following an exponential function from which a half-life for photodegradation ($\tau_{1/2}$) of 74 min can be determined. The luminescence intensity of $[Mo(L^3)_3]$ decreases only to 94% of its initial value in the same time period. From the two data sets in Figure 6 we calculate that the initial photodegradation rate (concentration change per unit time) of $[Mo(L^3)_3]$ in toluene is roughly a factor of 1300 lower than that for $[Ru(bpy)_3]^{2+}$ in acetonitrile under the high-power excitation conditions employed here (SI, page S30). Direct comparison of both complexes in the same solvent would be needed to make a truly quantitative statement concerning their relative inherent photostabilities, but the very disparate solubility characteristics of charge-neutral $[Mo(L^3)_3]$ and dicationic $[Ru(bpy)_3]^{2+}$ prohibit this. The main point here is the remarkably high photorobustness of $[Mo(L^3)_3]$ in toluene, the preferred solvent for the upconversion studies presented below. Based on our data, the quantum yield for photodegradation of $[Mo(L^3)_3]$ in toluene is only ca. 10^{-7} (SI page S31).

Triplet–Triplet Energy Transfer to DPA. With its triplet excited state at 1.77 eV,[114] DPA should be able to quench the

https://dx.doi.org/10.1021/jacs.0c12805
J. Am. Chem. Soc. 2021, 143, 1651−1663

^{3}MLCT luminescence of [Mo(L^3)$_3$] by triplet−triplet energy transfer (TTET). This is indeed the case (Figure 7A), and

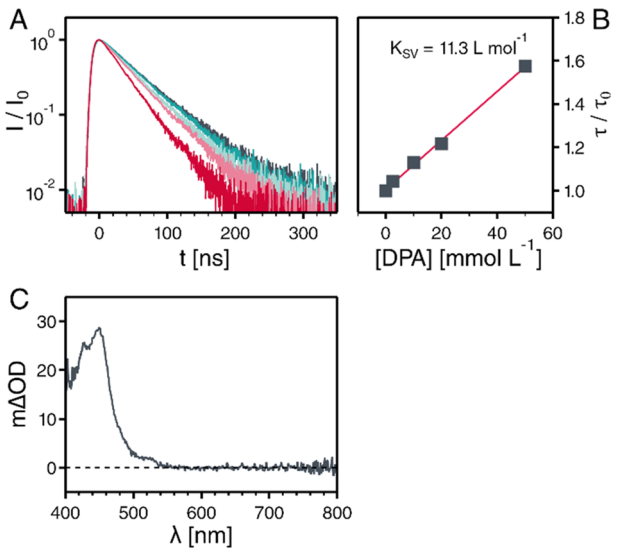

Figure 7. TTET from ^{3}MLCT-excited [Mo(L^3)$_3$] to DPA. (A) Decays of the ^{3}MLCT luminescence of 10−12 μM [Mo(L^3)$_3$] at 710 nm in deaerated toluene in absence (black trace) and in the presence of different DPA concentrations (colored traces). Excitation occurred at 532 nm with 20 mJ laser pulses of ca. 10 ns duration. (B) Stern−Volmer plot resulting from the data in (A). (C) Transient absorption spectrum recorded after 532 nm excitation of 12 μM [Mo(L^3)$_3$] in the presence of 50 mM DPA in deaerated toluene at 20 °C. The pulse duration was ca. 10 ns, the spectrum was recorded with a delay of 300 ns and time-integrated over an interval of 200 ns.

Stern−Volmer analysis of the DPA concentration-dependent ^{3}MLCT luminescence lifetime data in deaerated toluene (Figure 7B) yields a Stern−Volmer quenching constant (K_{SV}) of 11.3 M^{-1}. Transient absorption spectroscopy confirms that triplet-excited DPA (^{3}*DPA) is formed in this quenching process (Figure 7C), and there is no evidence for the formation of DPA radical ions;[115] hence, photoinduced electron transfer between [Mo(L^3)$_3$] and DPA is unimportant despite the high reducing power of photoexcited [Mo(L^3)$_3$] (−1.84 V vs SCE).[114] Based on τ_0 = 54 ns from the luminescence lifetime measurement by TCSPC (the value of 56 ns in Table 1 was determined by transient absorption spectroscopy) and K_{SV} = 11.3 M^{-1}, a rate constant (k_{TTET}) of (2.1 ± 0.2) × 10^8 M^{-1} s^{-1} is determined for TTET, which is roughly a factor of 50 below the diffusion limit for bimolecular reactions in toluene at 20 °C (1.1 × 10^{10} M^{-1} s^{-1}).[114] At the highest DPA concentration employed (50 mM, approaching the solubility limit), the ^{3}MLCT lifetime (τ) is reduced to 34.6 ns, and thus the TTET efficiency ($\eta_{TTET} = 1 - \tau/\tau_0$) becomes 0.36, whereas for a DPA concentration of 10 mM, η_{TTET} drops to 0.12. Rate constants for TTET can typically approach the diffusion limit when a driving force ($-\Delta G_{TTET}$) of ca. 0.2 eV is reached.[116] In our case, we estimate $\Delta G_{TTET} \approx -0.17$ eV, yet k_{TTET} is 50 times below the diffusion limit. We speculate that this could be due to the bulkiness of [Mo(L^3)$_3$], which might impede the formation of strong donor−acceptor orbital overlaps in the collisional encounter complex between [Mo(L^3)$_3$] and DPA.

Photochemical Upconversion. Photoexcitation of [Mo(L^3)$_3$] (11 μM) with a cw-laser at 635 nm in the presence of 10 mM DPA at various excitation densities results in the series of luminescence spectra shown in the left part of Figure 8A.

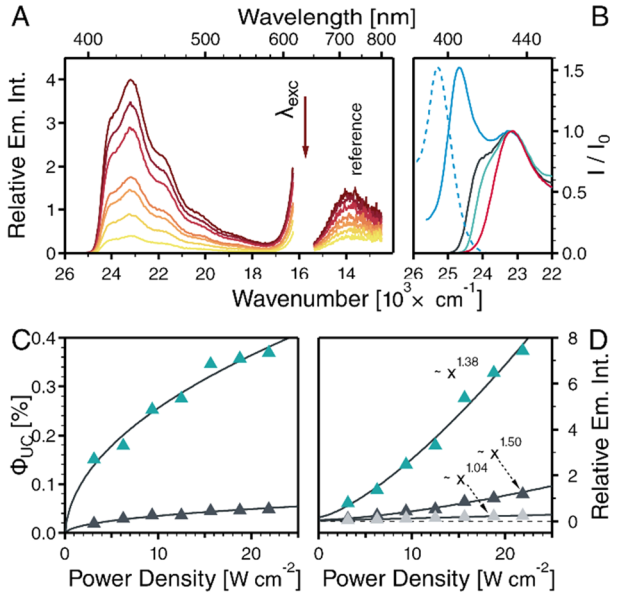

Figure 8. sTTA-UC. (A) Left: Delayed fluorescence after selective excitation of 11 μM [Mo(L^3)$_3$] in the presence of 2.5 mM DPA in deaerated toluene at 20 °C. Various power densities between 3 and 22 W/cm^2 were used for excitation at 635 nm. Right: Prompt ^{3}MLCT emission (scaled by a factor of approximately 10^{-2}) of 10 μM [Mo(L^3)$_3$] in deaerated toluene at 20 °C, containing no DPA but measured under otherwise strictly identical conditions as the delayed fluorescence spectra (see SI for details). (B) DPA fluorescence spectra as a function of DPA concentration (solid traces): 0.1 μM (blue), 2.5 mM (black), 10 mM (green), 50 mM (red). The dashed blue trace is an arbitrarily scaled absorption spectrum of DPA to help visualize the inner filter effect. (C) Upconversion efficiency as a function of excitation power density, as determined from eq 2 and the data in (A) for 2.5 mM DPA (black triangles) and an analogous data set obtained at 10 mM DPA concentration (green triangles). (D) Excitation power dependence of the delayed fluorescence intensity from (A) (2.5 mM DPA (black triangles)) and an analogous data set obtained at 10 mM DPA (green triangles). The gray triangles show the excitation power dependence of the [Mo(L^3)$_3$] ^{3}MLCT emission from the data set in (A).

The prominent band between 25 000 and 17 000 cm^{-1} is due to delayed fluorescence from DPA, while the band below 15 500 cm^{-1} is the unquenched ^{3}MLCT emission of [Mo(L^3)$_3$] in the absence of DPA but under otherwise strictly identical conditions. The latter spectra serve as reference points for the estimation of the upconversion efficiency, as discussed in detail further below. In time-resolved experiments using pulsed excitation at 532 nm, the DPA fluorescence decays on a time scale of several hundred microseconds in deaerated toluene at 20 °C, reflecting the 153 μs lifetime of the lowest DPA triplet excited state (^{3}*DPA) as determined by transient absorption spectroscopy (Figure S15). By contrast, the ^{3}MLCT emission of [Mo(L^3)$_3$] (τ_0 = 54 ns; see above) has decayed essentially completely after 300 ns (Figure 7A). The observation of a minor residual ^{3}MLCT luminescence signal beyond 300 ns (Figure S16) indicates that there is either some reverse TTET from ^{3}*DPA to [Mo(L^3)$_3$] or some reabsorption of DPA fluorescence by [Mo(L^3)$_3$] (or a combination of both), but these undesired processes are evidently very inefficient.

https://dx.doi.org/10.1021/jacs.0c12805
J. Am. Chem. Soc. 2021, 143, 1651−1663

The spectral shape of the DPA fluorescence is concentration dependent, and this is important for determination of the anti-Stokes shift. Upon direct excitation in highly dilute solution (solid blue trace in Figure 8B), the so-called 0−0 band at 405 nm is more prominent than all following progression members in a skeletal vibration mode and as such represents the emission band maximum. However, at the concentrations relevant to upconversion, the emission band maximum is at 430 nm due to an inner-filter effect attenuating the 0−0 band (black, green, and red traces in Figure 8B). Thus, based on an excitation wavelength of 635 nm and an emission band maximum at 430 nm, an anti-Stokes shift of 0.93 eV is obtained. This value compares favorably to the many sTTA-UC systems exhibiting anti-Stokes shifts in the range 0.4−0.8 eV.[76,117] Two recent studies claimed to observe greater anti-Stokes shifts with DPA (1.08 eV,[81] 1.14 eV[104]) despite very similar excitation wavelengths (665/663 nm). However, these estimates were based on the DPA fluorescence band maximum in very dilute solution, even though this is not the band maximum under upconversion conditions and consequently leads to an overestimation of the anti-Stokes shift. Using similar analysis, we would obtain a value of 1.11 eV. Other studies reported anti-Stokes shifts between 0.97 and 1.28 eV in systems with anthracene- and perylene-based annihilators,[74,118,119] and in a recently disclosed lanthanide-based upconversion system, an anti-Stokes shift of just less than 1 eV was found.[120] Against this background, it seems fair to state that the anti-Stokes shift of our $[Mo(L^3)_3]$/DPA combo is among the largest reported to date.

Integrated emission intensities from excitation power-dependent measurements with a 635 nm cw-laser are shown in Figure 8D. Expectedly, the ^{3}MLCT luminescence intensity increases linearly with increasing excitation power (gray triangles), whereas the upconverted DPA fluorescence intensity is best fitted to power functions yielding exponents between 1.38 and 1.50 (green and black triangles), depending on exact conditions. The significant deviation from quadratic power dependence is likely a manifestation of the fact that the system approaches the strong annihilation limit, in which the rate constant for TTA exceeds the rate constant for triplet−triplet energy transfer ($k_{TTA} > k_{TTET}$).[121] This hypothesis is supported by the finding of a higher exponent (n) at lower DPA concentration (n = 1.50 for 2.5 mM DPA, black triangles in Figure 8D, versus n = 1.38 for 10 mM DPA, green triangles). As noted in the previous section, k_{TTET} is roughly a factor of 50 below the diffusion limit, and this can help explain why the strong annihilation limit is apparently approached easily with the $[Mo(L^3)_3]$/DPA couple.

The quantum yield for upconversion (ϕ_{UC}) was determined with eq 2,[117] using as input data those from Figure 8A, i.e. the $[Mo(L^3)_3]$/DPA combo and a reference solution containing only $[Mo(L^3)_3]$ but no DPA. In that equation, Abs_{UC} and Abs_{ref} represent the absorbance of the two solutions at 635 nm, whereas I_{UC} and I_{ref} stand for the integrated DPA and ^{3}MLCT luminescence intensities of the two different solutions at a given excitation density. ϕ_{ref} is the ^{3}MLCT luminescence quantum yield of $[Mo(L^3)_3]$. Equation 2 is formulated such that a maximum value of 0.5 (i.e., 50%) can result for ϕ_{UC}.[117,122]

$$\phi_{UC} = \phi_{ref} \times (Abs_{ref}/Abs_{UC}) \times (I_{UC}/I_{ref}) \quad (2)$$

The outcome for two different annihilator concentrations and different excitation densities is shown in Figure 8C. At a DPA concentration of 10 mM, the highest achievable upconversion quantum yield is 0.0037 at an excitation power density of 22 W/cm^2, but under these conditions we were unable to reach the threshold power density (I_{th}) after which ϕ_{UC} reaches its true upper limit. However, when increasing the DPA concentration from 10 to 50 mM, ϕ_{UC} improves to 0.018 (Figure S21), mainly because the TTET efficiency (η_{TTET}) between ^{3}MLCT-excited $[Mo(L^3)_3]$ and DPA increases from 0.12 to 0.36 (see above). Thus, the achievable upconversion quantum yield of the $[Mo(L^3)_3]$/DPA combination approaches that of many sTTA-UC systems with precious metal-based sensitizers,[76] including some of the recently reported systems with record anti-Stokes shifts around 1 eV.[81,104,118−120] For instance, two Os-based systems yielded ϕ_{UC} = 0.050−0.055 (with a theoretical limit of 100%; in this case our ϕ_{UC} would be 0.036),[104,118] whereas Pd- and Pt-based systems gave ϕ_{UC} = 0.21−0.27.[81,119]

Given the need for high excitation densities for efficient sTTA-UC in most systems, the issue of long-term photostability under upconversion conditions is an important aspect. The inherent photostability of $[Mo(L^3)_3]$ under green light excitation is remarkably high (Figure 6), and the $[Mo(L^3)_3]$/DPA combo is also very robust under red light excitation (Figure 9). Using an excitation power density of 1.25 W/cm^2 at 635 nm to irradiate a deaerated toluene solution containing 13 μM $[Mo(L^3)_3]$ and 2 mM DPA at room temperature, the upconversion luminescence intensity at 430 nm was monitored as a function of time. Over the first 6 h, the signal decreases more or less linearly to 40% of its initial value, and over the following 10 h decays further to 9%. Thus, the upconversion system seems considerably less photorobust than $[Mo(L^3)_3]$ alone, though it should be kept in mind that excitation conditions to obtain the data sets in Figures 6 and 9 were different. Nevertheless, it seems plausible that the long-lived triplet excited state of DPA is particularly susceptible to undesired side reactions, and that the annihilator is therefore limiting the long-term performance of the overall system.

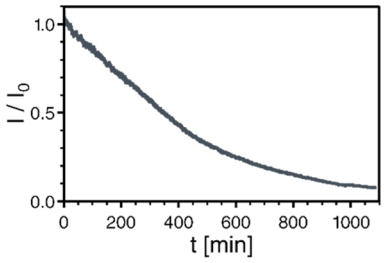

Figure 9. Photostability under upconversion conditions. Delayed fluorescence intensity emitted at 430 nm by a deaerated toluene solution of 13 μM $[Mo(L^3)_3]$ and 2 mM DPA in the course of cw-laser irradiation at 635 nm with a power density of 1.25 W/cm^2.

Photochemistry with Upconverted Light. In several recent studies, sTTA-UC was exploited to drive a photochemical reaction.[53,56,63,65,69,123−125] Performing a blue- or green-light dependent reaction in the same flask in which a sensitizer is excited with red light and the annihilator performs upconversion is a very elegant approach. Here, we aimed to explore a different concept, in which the upconversion and the blue-light-dependent photoreaction occur in spatially separate reaction vessels. Given the robustness of the $[Mo(L^3)_3]$/DPA system, we were curious whether its blue upconversion output could be sufficiently intense and durable to serve as a "blue

https://dx.doi.org/10.1021/jacs.0c12805
J. Am. Chem. Soc. 2021, 143, 1651−1663

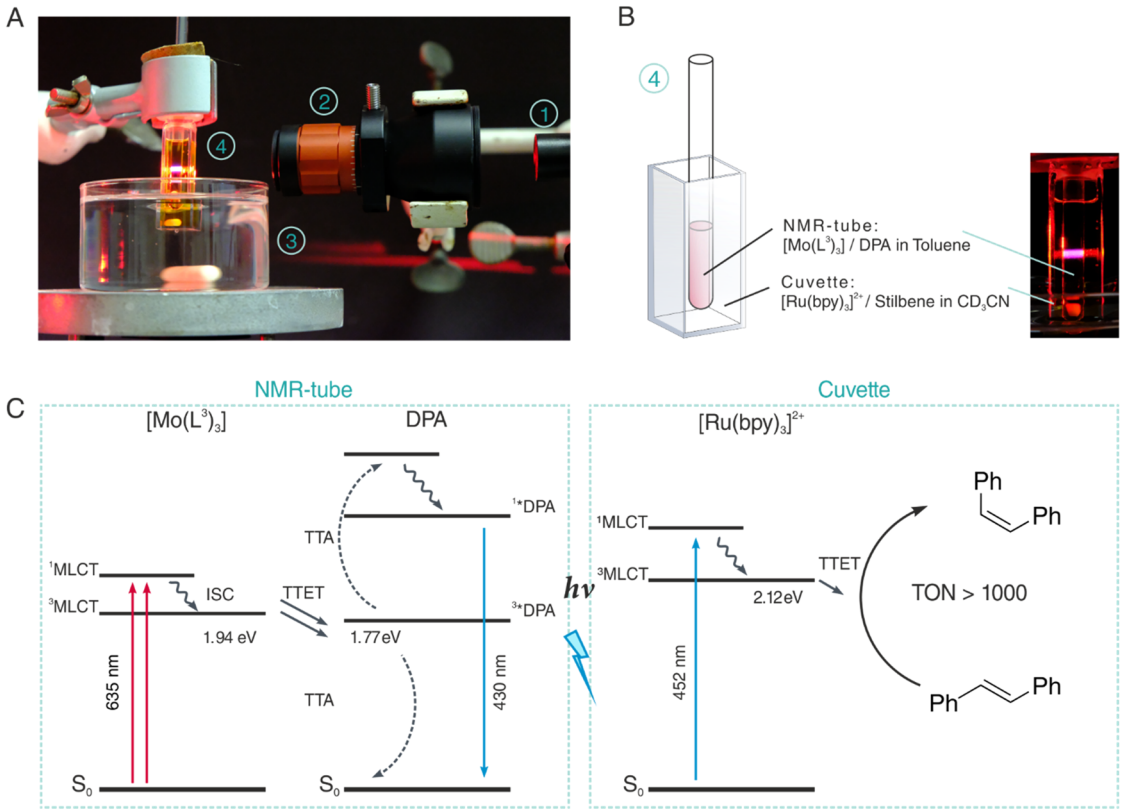

Figure 10. (A) Experimental setup for the photochemical isomerization of stilbene with upconverted light. The specific elements are (1) a red (635 nm) diode laser, (2) a beam expander used backward as an optical telescope, (3) a cooling bath with water, and (4) a quartz cuvette with the two spatially separate solutions, as illustrated in (B). A sealed NMR tube containing 13 μM $[Mo(L^3)_3]$ and 60 mM DPA in deaerated toluene is immersed into the cuvette containing 0.3 mM $[Ru(bpy)_3]^{2+}$ and 17 mM *trans*-stilbene in deaerated CD_3CN. Red-to-blue upconversion inside the NMR tube is visible by naked eye (right-hand side of (B)). (C) Operating principle of this setup: 635 nm excites exclusively $[Mo(L^3)_3]$ (penetrates the surrounding solution containing $[Ru(bpy)_3]^{2+}$), followed by intersystem crossing (ISC) and TTET to DPA. Triplet-excited DPA undergoes TTA and emits blue upconverted fluorescence. That 430 nm light passes across the NMR tube glass and excites $[Ru(bpy)_3]^{2+}$ in the surrounding solution. Following ISC and TTET to *trans*-stilbene, the substrate isomerizes to *cis*-stilbene.

lamp" for an NMR-scale reaction. Considering that many commercially available LEDs for photoredox catalysis have peak radiant fluxes on the order of 0.5 W/nm, it is not obvious that a photochemical upconversion system will provide sufficient photon flux and durability to drive a photochemical reaction requiring irradiation over several hours.

To test this concept, a solution of 13 μM $[Mo(L^3)_3]$ and 60 mM DPA in deaerated toluene was sealed in an NMR tube, which was immersed into a cuvette containing 0.3 mM $[Ru(bpy)_3]^{2+}$ and 17 mM *trans*-stilbene in deaerated CD_3CN (through an airtight rubber septum) as shown in Figure 10B. The $[Mo(L^3)_3]$ complex in the NMR tube was excited with a laser beam at 635 nm (Figure 10A), leading to red-to-blue upconversion that is detectable by the naked eye (right part of Figure 10B). The red excitation light easily penetrates through the surrounding $[Ru(bpy)_3]^{2+}$/stilbene solution in the cuvette, because the optical density of this reaction mixture at 635 nm is negligible.[126] However, the upconverted blue light is readily absorbed by $[Ru(bpy)_3]^{2+}$ ($\varepsilon_{430} \approx 14000\ M^{-1}\ cm^{-1}$,[126] present at 0.3 mM) in the cuvette surrounding the NMR tube. Intersystem crossing (ISC) and TTET lead to triplet-excited *trans*-stilbene, which can isomerize to *cis*-stilbene (Figure 10C).[127] After 17 h of irradiation at 635 nm, the yield of *cis*-stilbene was 50% (Figure 11B), while in the absence of light no conversion occurred at all (Figure 11A). When using a toluene solution containing the same concentration of $[Mo(L^3)_3]$ in the NMR tube, but no DPA, and irradiating at 635 nm for 17 h, only 5% of the *trans*-stilbene underwent isomerization (Figure 11C). This series of experiments clearly demonstrates the viability of the concept illustrated in Figure 10C.

The turnover number (TON) for the reaction mixture from Figure 11B is 1095 after 17 h of irradiation, calculated with respect to the $[Mo(L^3)_3]$ concentration (see SI pages S28–S29). According to the photostability data in Figure 9, the performance of the upconversion system decreases by 60% over the first 6 h. Consequently, when replacing the sTTA-UC system in the cuvette of Figure 10B after 5 h with a fresh solution of $[Mo(L^3)_3]$ and DPA, the overall reaction rate is improved, resulting in a similar TON (968) already after 10 h instead of 17 h.

The main purpose of the experiment in Figure 10 was to showcase the high performance and long-term robustness of the upconversion system based on an Earth-abundant metal complex, but the concept of using a photochemical upconversion system to drive a secondary light-dependent process in a separate reaction vessel might become interesting in broader contexts.[128−133] In particular, the spatial separation allows the formation of high-energy *triplets* from low-energy input light, instead of the high-energy *singlets* usually formed in sTTA-UC. In a one-pot reaction, the high-energy triplets (in our case the ^{3}MLCT excited state of $[Ru(bpy)_3]^{2+}$ at 2.12 eV) are expected to be quenched by the lower lying triplet states of

https://dx.doi.org/10.1021/jacs.0c12805
J. Am. Chem. Soc. 2021, 143, 1651−1663

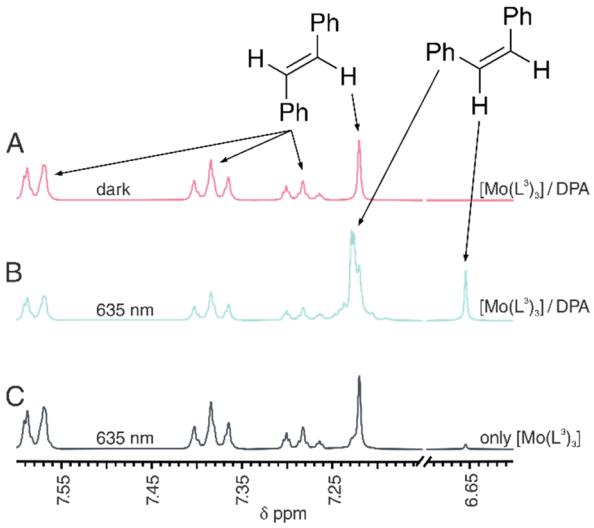

Figure 11. ^{1}H NMR spectra for the stilbene photoisomerization with upconverted light. A reaction mixture comprised of 0.3 mM $[Ru(bpy)_3]^{2+}$ and 17 mM *trans*-stilbene in CD_3CN was monitored under three different conditions in the reaction setup of Figure 10A/B: (A) The red laser remained switched off and the mixture stood in the dark for 17 h. (B) The upconversion system in the NMR tube comprised of 13 μM $[Mo(L^3)_3]$ and 60 mM DPA was irradiated at 635 nm for 17 h. (C) The NMR tube contained only 13 μM $[Mo(L^3)_3]$ (but no DPA) and was irradiated at 635 nm for 17 h.

the upconversion sensitizer (here the $[Mo(L^3)_3]$ complex with its lowest ^{3}MLCT state at 1.94 eV). Thus, the concept in Figure 10 might become useful for thermodynamically very challenging triplet photoreactions, and this seems noteworthy given the recent surge of interest in energy transfer catalysis.[3,134−142]

CONCLUSIONS

The incorporation of a thiophene bridging element and peripheral aryl substituents extending the overall π-conjugation of a chelating diisocyanide ligand (Scheme 1) gave access to a homoleptic Mo(0) complex emitting at more than 120 nm longer wavelengths than previously reported emissive Mo(0) complexes (Figure 3).[46,48] The photophysical properties of the latter resembled those of $[Ru(bpy)_3]^{2+}$, whereas the new $[Mo(L^3)_3]$ complex behaves more similarly to $[Os(bpy)_3]^{2+}$ concerning emission color, lifetime, and quantum yield. Thus, the diisocyanide chelate ligand design offers a tuning range that is comparable to a change in metal for homoleptic tris(bipyridine) complexes.

The $[Mo(L^3)_3]$ complex can be handled under an ambient atmosphere as a powder, and in deaerated toluene solution under photoirradiation it is remarkably robust (Figure 6). Temperature-dependent studies indicate that the thermal population of MC states from the luminescent ^{3}MLCT state can represent an important pathway for nonradiative relaxation in zerovalent group 6 metal complexes (Figure 5), from which one may conclude that future diisocyanide ligand designs should aim at further increasing the ligand field strength in order to maximize the ^{3}MLCT-MC energy gap.

The prior studies of photoactive Mo(0) complexes have focused largely on their use as strong reductants in photoredox catalysis,[46,48] whereas the present work shows that $[Mo(L^3)_3]$ is well suited for red-to-blue upconversion via triplet−triplet annihilation with 9,10-diphenylanthracene (Figure 8). Unlike in the case of Os(II) polypyridines, where red-light excitation for upconversion purposes occurs into a formally spin-forbidden singlet−triplet transition, $[Mo(L^3)_3]$ can be excited into a spin-allowed ^{1}MLCT absorption band at 635 nm (ε_{635} = 3340 M^{-1} cm^{-1}), and there is very little energy loss (0.012 eV) upon relaxation to the ^{3}MLCT state at 1.94 eV. The anti-Stokes shift of 0.93 eV for the $[Mo(L^3)_3]$/DPA couple is among the largest reported to date, and the upconversion quantum yield of 0.018 is similar to some Os(II)-based systems. The photorobustness under upconversion conditions with intense (500 mW) red diode laser excitation is remarkable and permits continued formation of blue output light over several hours (Figure 9). The upconverted blue photon flux is sufficiently high to drive a blue-light-dependent sensitized photoisomerization reaction in a separate reaction vessel (Figure 10). This concept of a photochemical upconversion system serving as a light source for a spatially separate reaction allows the formation of high energy *triplet* excited states from low energy triplets, whereas under ordinary sTTA-UC conditions only high energy *singlets* are formed. This opens new perspectives in multiphoton excitation chemistry.[69]

Our study illustrates that research on Earth-abundant alternatives for precious metal-based systems has much potential for unexpected discoveries and fundamentally new insights in photophysics and photochemistry, resonating with recent studies in this field.[16,17,28,29,38,143] This aspect seems equally important as the obvious economic and sustainability arguments associated with replacing precious metal complexes such as those based on Ru(II) and Os(II) with Earth-abundant transition metal compounds.

ASSOCIATED CONTENT

Supporting Information

The Supporting Information is available free of charge at https://pubs.acs.org/doi/10.1021/jacs.0c12805.

Synthetic protocols and characterization data, description of equipment and methods, supplementary electrochemical and spectroscopic data, details to upconversion quantum yield determination, details to photochemical experiments and photostability studies (PDF)

AUTHOR INFORMATION

Corresponding Author

Oliver S. Wenger − *Department of Chemistry, University of Basel, 4056 Basel, Switzerland;* orcid.org/0000-0002-0739-0553; Email: oliver.wenger@unibas.ch

Authors

Jakob B. Bilger − *Department of Chemistry, University of Basel, 4056 Basel, Switzerland*

Christoph Kerzig − *Department of Chemistry, University of Basel, 4056 Basel, Switzerland;* orcid.org/0000-0002-1026-1146

Christopher B. Larsen − *Department of Chemistry, University of Basel, 4056 Basel, Switzerland;* orcid.org/0000-0003-3006-2408

Complete contact information is available at: https://pubs.acs.org/10.1021/jacs.0c12805

Notes

The authors declare no competing financial interest.

https://dx.doi.org/10.1021/jacs.0c12805
J. Am. Chem. Soc. 2021, 143, 1651−1663

■ ACKNOWLEDGMENTS

This work was funded by the Swiss National Science Foundation through Grant Number 200021_178760 and through the NCCR Molecular Systems Engineering. C.K. acknowledges a Novartis University of Basel Excellence Scholarship for Life Sciences by the Research Fund of the University of Basel. This work is dedicated to Professor Wolfgang Kaim on the occasion of his 70th birthday.

■ REFERENCES

(1) Juris, A.; Balzani, V.; Barigelletti, F.; Campagna, S.; Belser, P.; Von Zelewsky, A. Ru(II) Polypyridine Complexes - Photophysics, Photochemistry, Electrochemistry, and Chemi-Luminescence. *Coord. Chem. Rev.* **1988**, *84*, 85−277.
(2) Twilton, J.; Le, C.; Zhang, P.; Shaw, M. H.; Evans, R. W.; MacMillan, D. W. C. The merger of transition metal and photocatalysis. *Nat. Rev. Chem.* **2017**, *1*, 0052.
(3) Strieth-Kalthoff, F.; James, M. J.; Teders, M.; Pitzer, L.; Glorius, F. Energy transfer catalysis mediated by visible light: principles, applications, directions. *Chem. Soc. Rev.* **2018**, *47*, 7190−7202.
(4) Yersin, H.; Rausch, A. F.; Czerwieniec, R.; Hofbeck, T.; Fischer, T. The Triplet State of Organo-Transition Metal Compounds. Triplet Harvesting and Singlet Harvesting for Efficient OLEDs. *Coord. Chem. Rev.* **2011**, *255*, 2622−2652.
(5) Mills, I. N.; Porras, J. A.; Bernhard, S. Judicious Design of Cationic, Cyclometalated Ir^{III} Complexes for Photochemical Energy Conversion and Optoelectronics. *Acc. Chem. Res.* **2018**, *51*, 352−364.
(6) Hammarström, L. Accumulative Charge Separation for Solar Fuels Production: Coupling Light-Induced Single Electron Transfer to Multielectron Catalysis. *Acc. Chem. Res.* **2015**, *48*, 840−850.
(7) Morris, A. J.; Meyer, G. J.; Fujita, E. Molecular Approaches to the Photocatalytic Reduction of Carbon Dioxide for Solar Fuels. *Acc. Chem. Res.* **2009**, *42*, 1983−1994.
(8) Bevernaegie, R.; Wehlin, S. A. M.; Piechota, E. J.; Abraham, M.; Philouze, C.; Meyer, G. J.; Elias, B.; Troian-Gautier, L. Improved Visible Light Absorption of Potent Iridium(III) Photo-oxidants for Excited-State Electron Transfer Chemistry. *J. Am. Chem. Soc.* **2020**, *142*, 2732−2737.
(9) Heinemann, F.; Karges, J.; Gasser, G. Critical overview of the use of Ru(II) polypyridyl complexes as photosensitizers in one-photon and two-photon photodynamic therapy. *Acc. Chem. Res.* **2017**, *50*, 2727−2736.
(10) White, J. K.; Schmehl, R. H.; Turro, C. An overview of photosubstitution reactions of Ru(II) imine complexes and their application in photobiology and photodynamic therapy. *Inorg. Chim. Acta* **2017**, *454*, 7−20.
(11) Auböck, G.; Chergui, M. Sub-50-fs photoinduced spin crossover in $Fe(bpy_3)^{2+}$. *Nat. Chem.* **2015**, *7*, 629−633.
(12) Ashley, D. C.; Jakubikova, E. Ironing out the Photochemical and Spin-Crossover Behavior of Fe(II) Coordination Compounds with Computational Chemistry. *Coord. Chem. Rev.* **2017**, *337*, 97−111.
(13) Armaroli, N. Photoactive Mono- and Polynuclear Cu^{I}-Phenanthrolines. A Viable Alternative to Ru^{II}-Polypyridines? *Chem. Soc. Rev.* **2001**, *30*, 113−124.
(14) Lazorski, M. S.; Castellano, F. N. Advances in the Light Conversion Properties of Cu(I)-Based Photosensitizers. *Polyhedron* **2014**, *82*, 57−70.
(15) Zhang, W. K.; Gaffney, K. J. Mechanistic Studies of Photoinduced Spin Crossover and Electron Transfer in Inorganic Complexes. *Acc. Chem. Res.* **2015**, *48*, 1140−1148.
(16) Hamze, R.; Peltier, J. L.; Sylvinson, D.; Jung, M.; Cardenas, J.; Haiges, R.; Soleilhavoup, M.; Jazzar, R.; Djurovich, P. I.; Bertrand, G.; Thompson, M. E. Eliminating nonradiative decay in Cu^{I} emitters: > 99% quantum efficiency and microsecond lifetime. *Science* **2019**, *363*, 601−606.
(17) Gernert, M.; Balles-Wolf, L.; Kerner, F.; Müller, U.; Schmiedel, A.; Holzapfel, M.; Marian, C. M.; Pflaum, J.; Lambert, C.; Steffen, A. Cyclic (amino)(aryl)carbenes enter the field of chromophore ligands: expanded π system leads to unusually deep red emitting Cu^{I} compounds. *J. Am. Chem. Soc.* **2020**, *142*, 8897−8909.
(18) Di, D. W.; Romanov, A. S.; Yang, L.; Richter, J. M.; Rivett, J. P. H.; Jones, S.; Thomas, T. H.; Jalebi, M. A.; Friend, R. H.; Linnolahti, M.; Bochmann, M.; Credgington, D. High-performance light-emitting diodes based on carbene-metal-amides. *Science* **2017**, *356*, 159−163.
(19) Hossain, A.; Bhattacharyya, A.; Reiser, O. Copper's rapid ascent in visible-light photoredox catalysis. *Science* **2019**, *364*, 450−461.
(20) Shepard, S. G.; Fatur, S. M.; Rappe, A. K.; Damrauer, N. H. Highly Strained Iron(II) Polypyridines: Exploiting the Quintet Manifold To Extend the Lifetime of MLCT Excited States. *J. Am. Chem. Soc.* **2016**, *138*, 2949−2952.
(21) Zhang, K.; Ash, R.; Girolami, G. S.; Vura-Weis, J. Tracking the metal-centered triplet in photoinduced spin crossover of $Fe(phen)_3^{2+}$ with tabletop femtosecond M-edge X-ray absorption near-edge structure spectroscopy. *J. Am. Chem. Soc.* **2019**, *141*, 17180−17188.
(22) Vukadinovic, Y.; Burkhardt, L.; Papcke, A.; Miletic, A.; Fritsch, L.; Altenburger, B.; Schoch, R.; Neuba, A.; Lochbrunner, S.; Bauer, M. When Donors Turn into Acceptors: Ground and Excited State Properties of Fe^{II} Complexes with Amine-Substituted Tridentate Bisimidazole-2-ylidene Pyridine Ligands. *Inorg. Chem.* **2020**, *59*, 8762−8774.
(23) Förster, C.; Heinze, K. Photophysics and photochemistry with earth-abundant metals − fundamentals and concepts. *Chem. Soc. Rev.* **2020**, *49*, 1057−1070.
(24) Duchanois, T.; Liu, L.; Pastore, M.; Monari, A.; Cebrian, C.; Trolez, Y.; Darari, M.; Magra, K.; Frances-Monerris, A.; Domenichini, E.; Beley, M.; Assfeld, X.; Haacke, S.; Gros, P. C. NHC-based iron sensitizers for DSSCs. *Inorganics* **2018**, *6*, 63.
(25) Liu, Y. Z.; Persson, P.; Sundström, V.; Wärnmark, K. Fe N-heterocyclic carbene complexes as promising photosensitizers. *Acc. Chem. Res.* **2016**, *49*, 1477−1485.
(26) Nicholls, T. P.; Bissember, A. C. Developments in visible-light-mediated copper photocatalysis. *Tetrahedron Lett.* **2019**, *60*, 150883.
(27) Wenger, O. S. Photoactive Complexes with Earth-Abundant Metals. *J. Am. Chem. Soc.* **2018**, *140*, 13522−13533.
(28) Kjær, K. S.; Kaul, N.; Prakash, O.; Chábera, P.; Rosemann, N. W.; Honarfar, A.; Gordivska, O.; Fredin, L. A.; Bergquist, K. E.; Häggström, L.; Ericsson, T.; Lindh, L.; Yartsev, A.; Styring, S.; Huang, P.; Uhlig, J.; Bendix, J.; Strand, D.; Sundström, V.; Persson, P.; Lomoth, R.; Wärnmark, K. Luminescence and reactivity of a charge-transfer excited iron complex with nanosecond lifetime. *Science* **2019**, *363*, 249−253.
(29) Zhang, Y.; Lee, T. S.; Favale, J. M.; Leary, D. C.; Petersen, J. L.; Scholes, G. D.; Castellano, F. N.; Milsmann, C. Delayed fluorescence from a zirconium(IV) photosensitizer with ligand-to-metal charge-transfer excited states. *Nat. Chem.* **2020**, *12*, 345−352.
(30) Pal, A. K.; Li, C. F.; Hanan, G. S.; Zysman-Colman, E. Blue-emissive cobalt(III) complexes and their use in the photocatalytic trifluoromethylation of polycyclic aromatic hydrocarbons. *Angew. Chem., Int. Ed.* **2018**, *57*, 8027−8031.
(31) Harris, J. P.; Reber, C.; Colmer, H. E.; Jackson, T. A.; Forshaw, A. P.; Smith, J. M.; Kinney, R. A.; Telser, J. Near-infrared $^2E_g \rightarrow {}^4A_{2g}$ and visible LMCT luminescence from a molecular bis-(tris(carbene)-borate) manganese(IV) complex. *Can. J. Chem.* **2017**, *95*, 547−552.
(32) Wong, Y. S.; Tang, M. C.; Ng, M. G.; Yam, V. W. W. Toward the Design of Phosphorescent Emitters of Cyclometalated Earth-Abundant Nickel(II) and Their Supramolecular Study. *J. Am. Chem. Soc.* **2020**, *142*, 7638−7646.
(33) Chan, K. T.; Lam, T. L.; Yu, D. H.; Du, L.; Phillips, D. L.; Kwong, C. L.; Tong, G. S. M.; Cheng, G.; Che, C. M. Strongly Luminescent Tungsten Emitters with Emission Quantum Yields of up to 84%: TADF and High-Efficiency Molecular Tungsten OLEDs. *Angew. Chem., Int. Ed.* **2019**, *58*, 14896−14900.
(34) Otto, S.; Dorn, M.; Förster, C.; Bauer, M.; Seitz, M.; Heinze, K. Understanding and Exploiting Long-Lived Near-Infrared Emission of a Molecular Ruby. *Coord. Chem. Rev.* **2018**, *359*, 102−111.

https://dx.doi.org/10.1021/jacs.0c12805
J. Am. Chem. Soc. 2021, 143, 1651−1663

(35) Ting, S. I.; Garakyaraghi, S.; Taliaferro, C. M.; Shields, B. J.; Scholes, G. D.; Castellano, F. N.; Doyle, A. G. ^{3}d-d Excited States of Ni(II) Complexes Relevant to Photoredox Catalysis: Spectroscopic Identification and Mechanistic Implications. *J. Am. Chem. Soc.* **2020**, *142*, 5800−5810.
(36) Yin, H. L.; Carroll, P. J.; Anna, J. M.; Schelter, E. J. Luminescent Ce^{III} Complexes as Stoichiometric and Catalytic Photoreductants for Halogen Atom Abstraction Reactions. *J. Am. Chem. Soc.* **2015**, *137*, 9234−9237.
(37) Jimenez, J. R.; Doistau, B.; Cruz, C. M.; Besnard, C.; Cuerva, J. M.; Campana, A. G.; Piguet, C. Chiral Molecular Ruby $[Cr(dqp)_2]^{3+}$ with Long-Lived Circularly Polarized Luminescence. *J. Am. Chem. Soc.* **2019**, *141*, 13244−13252.
(38) Dorn, M.; Kalmbach, J.; Boden, P.; Päpcke, A.; Gómez, S.; Förster, C.; Kuczelinis, F.; Carrella, L. M.; Büldt, L. A.; Bings, N. H.; Rentschler, E.; Lochbrunner, S.; González, L.; Gerhards, M.; Seitz, M.; Heinze, K. A Vanadium(III) Complex with Blue and NIR-II Spin-Flip Luminescence in Solution. *J. Am. Chem. Soc.* **2020**, *142*, 7947−7955.
(39) Dill, R. D.; Portillo, R. I.; Shepard, S. G.; Shores, M. P.; Rappé, A. K.; Damrauer, N. H. Long-Lived Mixed ^{2}MLCT/MC States in Antiferromagnetically Coupled d^3 Vanadium(II) Bipyridine and Phenanthroline Complexes. *Inorg. Chem.* **2020**, *59*, 14706−14715.
(40) Grübel, M.; Bosque, I.; Altmann, P. J.; Bach, T.; Hess, C. R. Redox and Photocatalytic Properties of a Ni^{II} Complex with a Macrocyclic Biquinazoline (Mabiq) Ligand. *Chem. Sci.* **2018**, *9*, 3313−3317.
(41) Mann, K. R.; Cimolino, M.; Geoffroy, G. L.; Hammond, G. S.; Orio, A. A.; Albertin, G.; Gray, H. B. Electronic structures and spectra of hexakisphenylisocyanide complexes of Cr^0, Mo^0, W^0, Mn^I, and Mn^{II}. *Inorg. Chim. Acta* **1976**, *16*, 97−101.
(42) Mann, K. R.; Gray, H. B.; Hammond, G. S. Excited-state reactivity patterns of hexakisarylisocyano complexes of chromium(0), molybdenum(0), and tungsten(0). *J. Am. Chem. Soc.* **1977**, *99*, 306−307.
(43) Sattler, W.; Ener, M. E.; Blakemore, J. D.; Rachford, A. A.; LaBeaume, P. J.; Thackeray, J. W.; Cameron, J. F.; Winkler, J. R.; Gray, H. B. Generation of Powerful Tungsten Reductants by Visible Light Excitation. *J. Am. Chem. Soc.* **2013**, *135*, 10614−10617.
(44) Sattler, W.; Henling, L. M.; Winkler, J. R.; Gray, H. B. Bespoke photoreductants: tungsten arylisocyanides. *J. Am. Chem. Soc.* **2015**, *137*, 1198−1205.
(45) Fajardo, J.; Schwan, J.; Takase, M. K.; Winkler, J. R.; Gray, H. B. Third Generation $W(CNAr)_6$ Photoreductants (CNAr = Fused-Ring and Alkynyl-Bridged Arylisocyanides). *Inorg. Chem.* **2020**, DOI: 10.1021/acs.inorgchem.0c02912.
(46) Büldt, L. A.; Guo, X.; Prescimone, A.; Wenger, O. S. A Molybdenum(0) Isocyanide Analogue of Ru(2,2′-Bipyridine)$_3^{2+}$: A Strong Reductant for Photoredox Catalysis. *Angew. Chem., Int. Ed.* **2016**, *55*, 11247−11250.
(47) Büldt, L. A.; Guo, X.; Vogel, R.; Prescimone, A.; Wenger, O. S. A tris(diisocyanide)chromium(0) complex is a luminescent analog of Fe(2,2′-bipyridine)$_3^{2+}$. *J. Am. Chem. Soc.* **2017**, *139*, 985−992.
(48) Herr, P.; Glaser, F.; Büldt, L. A.; Larsen, C. B.; Wenger, O. S. Long-lived, strongly emissive, and highly reducing excited states in Mo(0) complexes with chelating isocyanides. *J. Am. Chem. Soc.* **2019**, *141*, 14394−14402.
(49) Garakyaraghi, S.; McCusker, C. E.; Khan, S.; Koutnik, P.; Bui, A. T.; Castellano, F. N. Enhancing the Visible-Light Absorption and Excited-State Properties of Cu(I) MLCT Excited States. *Inorg. Chem.* **2018**, *57*, 2296−2307.
(50) Wieghold, S.; Bieber, A. S.; VanOrman, Z. A.; Daley, L.; Leger, M.; Correa-Baena, J.-P.; Nienhaus, L. Triplet Sensitization by Lead Halide Perovskite Thin Films for Efficient Solid-State Photon Upconversion at Subsolar Fluxes. *Matter* **2019**, *1*, 705−719.
(51) Bonnet, S. Shifting the Light Activation of Metallodrugs to the Red and Near-Infrared Region in Anticancer Phototherapy. *Comments Inorg. Chem.* **2015**, *35*, 179−213.
(52) Cerfontaine, S.; Wehlin, S. A. M.; Elias, B.; Troian-Gautier, L. Photostable Polynuclear Ruthenium(II) Photosensitizers Competent for Dehalogenation Photoredox Catalysis at 590 nm. *J. Am. Chem. Soc.* **2020**, *142*, 5549−5555.
(53) Tokunaga, A.; Uriarte, L. M.; Mutoh, K.; Fron, E.; Hofkens, J.; Sliwa, M.; Abe, J. Photochromic Reaction by Red Light via Triplet Fusion Upconversion. *J. Am. Chem. Soc.* **2019**, *141*, 17744−17753.
(54) Askes, S. H. C.; Meijer, M. S.; Bouwens, T.; Landman, I.; Bonnet, S. Red Light Activation of Ru(II) Polypyridyl Prodrugs via Triplet-Triplet Annihilation Upconversion: Feasibility in Air and through Meat. *Molecules* **2016**, *21*, 1460.
(55) Huang, L.; Wu, W.; Li, Y.; Huang, K.; Zeng, L.; Lin, W.; Han, G. Highly Effective Near-Infrared Activating Triplet−Triplet Annihilation Upconversion for Photoredox Catalysis. *J. Am. Chem. Soc.* **2020**, *142*, 18460−18470.
(56) Ravetz, B. D.; Tay, N. E. S.; Joe, C. L.; Sezen-Edmonds, M.; Schmidt, M. A.; Tan, Y.; Janey, J. M.; Eastgate, M. D.; Rovis, T. Development of a Platform for Near-Infrared Photoredox Catalysis. *ACS Cent. Sci.* **2020**, *6*, 2053−2059.
(57) Kerzig, C.; Goez, M. Combining Energy and Electron Transfer in a Supramolecular Environment for the "Green" Generation and Utilization of Hydrated Electrons through Photoredox Catalysis. *Chem. Sci.* **2016**, *7*, 3862−3868.
(58) Zeng, L.; Liu, T.; He, C.; Shi, D. Y.; Zhang, F. L.; Duan, C. Y. Organized Aggregation Makes Insoluble Perylene Diimide Efficient for the Reduction of Aryl Halides via Consecutive Visible Light-Induced Electron-Transfer Processes. *J. Am. Chem. Soc.* **2016**, *138*, 3958−3961.
(59) Zeman, C. J.; Kim, S.; Zhang, F.; Schanze, K. S. Direct Observation of the Reduction of Aryl Halides by a Photoexcited Perylene Diimide Radical Anion. *J. Am. Chem. Soc.* **2020**, *142*, 2204−2207.
(60) Marchini, M.; Gualandi, A.; Mengozzi, L.; Franchi, P.; Lucarini, M.; Cozzi, P. G.; Balzani, V.; Ceroni, P. Mechanistic Insights into Two-Photon-Driven Photocatalysis in Organic Synthesis. *Phys. Chem. Chem. Phys.* **2018**, *20*, 8071−8076.
(61) Ghosh, I.; Ghosh, T.; Bardagi, J. I.; König, B. Reduction of Aryl Halides by Consecutive Visible Light-Induced Electron Transfer Processes. *Science* **2014**, *346*, 725−728.
(62) Coles, M. S.; Quach, G.; Beves, J. E.; Moore, E. G. A Photophysical Study of Sensitization-Initiated Electron Transfer: Insights into the Mechanism of Photoredox Activity. *Angew. Chem., Int. Ed.* **2020**, *59*, 9522−9526.
(63) Majek, M.; Faltermeier, U.; Dick, B.; Pérez-Ruiz, R.; Jacobi von Wangelin, A. Application of Visible-to-UV Photon Upconversion to Photoredox Catalysis: The Activation of Aryl Bromides. *Chem. - Eur. J.* **2015**, *21*, 15496−15501.
(64) Connell, T. U.; Fraser, C. L.; Czyz, M. L.; Smith, Z. M.; Hayne, D. J.; Doeven, E. H.; Agugiaro, J.; Wilson, D. J. D.; Adcock, J. L.; Scully, A. D.; Gomez, D. E.; Barnett, N. W.; Polyzos, A.; Francis, P. S. The Tandem Photoredox Catalysis Mechanism of $[Ir(ppy)_2(dtb\text{-}bpy)]^+$ Enabling Access to Energy Demanding Organic Substrates. *J. Am. Chem. Soc.* **2019**, *141*, 17646−17658.
(65) Ravetz, B. D.; Pun, A. B.; Churchill, E. M.; Congreve, D. N.; Rovis, T.; Campos, L. M. Photoredox catalysis using infrared light via triplet fusion upconversion. *Nature* **2019**, *565*, 343−346.
(66) Gray, V.; Dzebo, D.; Abrahamsson, M.; Albinsson, B.; Moth-Poulsen, K. Triplet−triplet annihilation photon-upconversion: towards solar energy applications. *Phys. Chem. Chem. Phys.* **2014**, *16*, 10345−10352.
(67) Pfund, B.; Steffen, D. M.; Schreier, M. R.; Bertrams, M. S.; Ye, C.; Börjesson, K.; Wenger, O. S.; Kerzig, C. UV Light Generation and Challenging Photoreactions Enabled by Upconversion in Water. *J. Am. Chem. Soc.* **2020**, *142*, 10468−10476.
(68) Rauch, M. P.; Knowles, R. R. Applications and Prospects for Triplet-Triplet Annihilation Photon Upconversion. *Chimia* **2018**, *72*, 501−507.

https://dx.doi.org/10.1021/jacs.0c12805
J. Am. Chem. Soc. 2021, 143, 1651−1663

(69) Glaser, F.; Kerzig, C.; Wenger, O. S. Multi-Photon Excitation in Photoredox Catalysis: Concepts, Applications, Methods. *Angew. Chem., Int. Ed.* **2020**, *59*, 10266−10284.
(70) Caspar, J. V.; Meyer, T. J. Application of the Energy-Gap Law to Nonradiative Excited-State Decay. *J. Phys. Chem.* **1983**, *87*, 952−957.
(71) Amemori, S.; Sasaki, Y.; Yanai, N.; Kimizuka, N. Near-Infrared-to-Visible Photon Upconversion Sensitized by a Metal Complex with Spin-Forbidden yet Strong S_0-T_1 Absorption. *J. Am. Chem. Soc.* **2016**, *138*, 8702−8705.
(72) Liu, D.; Zhao, Y.; Wang, Z.; Xu, K.; Zhao, J. Exploiting the benefit of $S_0 \rightarrow T_1$ excitation in triplet−triplet annihilation upconversion to attain large anti-stokes shifts: tuning the triplet state lifetime of a tris(2,2′-bipyridine) osmium(II) complex. *Dalton Trans.* **2018**, *47*, 8619−8628.
(73) Sasaki, Y.; Oshikawa, M.; Bharmoria, P.; Kouno, H.; Hayashi-Takagi, A.; Sato, M.; Ajioka, I.; Yanai, N.; Kimizuka, N. Near-Infrared Optogenetic Genome Engineering Based on Photon-Upconversion Hydrogels. *Angew. Chem., Int. Ed.* **2019**, *58*, 17827−17833.
(74) Sasaki, Y.; Amemori, S.; Kouno, H.; Yanai, N.; Kimizuka, N. Near infrared-to-blue photon upconversion by exploiting direct S-T absorption of a molecular sensitizer. *J. Mater. Chem. C* **2017**, *5*, 5063−5067.
(75) Islangulov, R. R.; Lott, J.; Weder, C.; Castellano, F. N. Noncoherent low-power upconversion in solid polymer films. *J. Am. Chem. Soc.* **2007**, *129*, 12652−12653.
(76) Bharmoria, P.; Bildirir, H.; Moth-Poulsen, K. Triplet-triplet annihilation based near infrared to visible molecular photon upconversion. *Chem. Soc. Rev.* **2020**, *49*, 6529−6554.
(77) Rowe, J. M.; Zhu, J.; Soderstrom, E. M.; Xu, W. Q.; Yakovenko, A.; Morris, A. J. Sensitized photon upconversion in anthracene-based zirconium metal-organic frameworks. *Chem. Commun.* **2018**, *54*, 7798−7801.
(78) Nattestad, A.; Cheng, Y. Y.; MacQueen, R. W.; Schulze, T. F.; Thompson, F. W.; Mozer, A. J.; Fückel, B.; Khoury, T.; Crossley, M. J.; Lips, K.; Wallace, G. G.; Schmidt, T. W. Dye-Sensitized Solar Cell with Integrated Triplet−Triplet Annihilation Upconversion System. *J. Phys. Chem. Lett.* **2013**, *4*, 2073−2078.
(79) Fallon, K. J.; Churchill, E. M.; Sanders, S. N.; Shee, J.; Weber, J. L.; Meir, R.; Jockusch, S.; Reichman, D. R.; Sfeir, M. Y.; Congreve, D. N.; Campos, L. M. Molecular Engineering of Chromophores to Enable Triplet−Triplet Annihilation Upconversion. *J. Am. Chem. Soc.* **2020**, *142*, 19917−19925.
(80) Graham, K. R.; Yang, Y. X.; Sommer, J. R.; Shelton, A. H.; Schanze, K. S.; Xue, J. G.; Reynolds, J. R. Extended Conjugation Platinum(II) Porphyrins for use in Near-Infrared Emitting Organic Light Emitting Diodes. *Chem. Mater.* **2011**, *23*, 5305−5312.
(81) Fan, C.; Wei, L.; Niu, T.; Rao, M.; Cheng, G.; Chruma, J. J.; Wu, W.; Yang, C. Efficient Triplet−Triplet Annihilation Upconversion with an Anti-Stokes Shift of 1.08 eV Achieved by Chemically Tuning Sensitizers. *J. Am. Chem. Soc.* **2019**, *141*, 15070−15077.
(82) Gray, V.; Moth-Poulsen, K.; Albinsson, B.; Abrahamsson, M. Towards efficient solid-state triplet−triplet annihilation based photon upconversion: Supramolecular, macromolecular and self-assembled systems. *Coord. Chem. Rev.* **2018**, *362*, 54−71.
(83) McCusker, C. E.; Castellano, F. N. Efficient Visible to Near-UV Photochemical Upconversion Sensitized by a Long Lifetime Cu(I) MLCT Complex. *Inorg. Chem.* **2015**, *54*, 6035−6042.
(84) Felter, K. M.; Fravventura, M. C.; Koster, E.; Abellon, R. D.; Savenije, T. J.; Grozema, F. C. Solid-State Infrared Upconversion in Perylene Diimides Followed by Direct Electron Injection. *ACS Energy Lett.* **2020**, *5*, 124−129.
(85) Sugunan, S. K.; Tripathy, U.; Brunet, S. M. K.; Paige, M. F.; Steer, R. P. Mechanisms of Low-Power Noncoherent Photon Upconversion in Metalloporphyrin−Organic Blue Emitter Systems in Solution. *J. Phys. Chem. A* **2009**, *113*, 8548−8556.
(86) Zhou, J.; Liu, Q.; Feng, W.; Sun, Y.; Li, F. Upconversion Luminescent Materials: Advances and Applications. *Chem. Rev.* **2015**, *115*, 395−465.
(87) Speckmeier, E.; Fischer, T. G.; Zeitler, K. A Toolbox Approach to Construct Broadly Applicable Metal-Free Catalysts for Photoredox Chemistry: Deliberate Tuning of Redox Potentials and Importance of Halogens in Donor-Acceptor Cyanoarenes. *J. Am. Chem. Soc.* **2018**, *140*, 15353−15365.
(88) McCarthy, B. G.; Pearson, R. M.; Lim, C. H.; Sartor, S. M.; Damrauer, N. H.; Miyake, G. M. Structure-Property Relationships for Tailoring Phenoxazines as Reducing Photoredox Catalysts. *J. Am. Chem. Soc.* **2018**, *140*, 5088−5101.
(89) White, A. R.; Wang, L. F.; Nicewicz, D. A. Synthesis and Characterization of Acridinium Dyes for Photoredox Catalysis. *Synlett* **2019**, *30*, 827−832.
(90) Congrave, D. G.; Drummond, B. H.; Conaghan, P. J.; Francis, H.; Jones, S. T. E.; Grey, C. P.; Greenham, N. C.; Credgington, D.; Bronstein, H. A Simple Molecular Design Strategy for Delayed Fluorescence toward 1000 nm. *J. Am. Chem. Soc.* **2019**, *141*, 18390−18394.
(91) Singh, V. K.; Yu, C.; Badgujar, S.; Kim, Y.; Kwon, Y.; Kim, D.; Lee, J.; Akhter, T.; Thangavel, G.; Park, L. S.; Lee, J.; Nandajan, P. C.; Wannemacher, R.; Milian-Medina, B.; Luer, L.; Kim, K. S.; Gierschner, J.; Kwon, M. S. Highly efficient organic photocatalysts discovered via a computer-aided-design strategy for visible-light-driven atom transfer radical polymerization. *Nat. Catal.* **2018**, *1*, 794−804.
(92) Dell'Amico, L.; Vega-Penaloza, A.; Mateos, J.; Companyo, X.; Escudero-Casao, M., A Rational Approach to Organo-Photocatalysis. Novel Designs and Structure−Property Relationships. *Angew. Chem., Int. Ed.* **2020**, DOI: 10.1002/anie.202006416.
(93) Manna, M. K.; Shokri, S.; Wiederrecht, G. P.; Gosztola, D. J.; Ayitou, A. J.-L. New perspectives for triplet−triplet annihilation based photon upconversion using all-organic energy donor & acceptor chromophores. *Chem. Commun.* **2018**, *54*, 5809−5818.
(94) Singh-Rachford, T. N.; Haefele, A.; Ziessel, R.; Castellano, F. N. Boron Dipyrromethene Chromophores: Next Generation Triplet Acceptors/Annihilators for Low Power Upconversion Schemes. *J. Am. Chem. Soc.* **2008**, *130*, 16164−16165.
(95) Murakami, Y.; Motooka, A.; Enomoto, R.; Niimi, K.; Kaiho, A.; Kiyoyanagi, N. Visible-to-ultraviolet (<340 nm) photon upconversion by triplet−triplet annihilation in solvents. *Phys. Chem. Chem. Phys.* **2020**, *22*, 27134−27143.
(96) Borikar, S. P.; Daniel, T.; Paul, V. Mild, Efficient, and Regioselective Monobromination of Arylamines and Phenols Using $[BBIm]Br_3$ as a New Reagent. *Synth. Commun.* **2010**, *40*, 647−653.
(97) Azizi, N.; Shirdel, F. Sustainable and chemoselective N-Boc protection of amines in biodegradable deep eutectic solvent. *Monatsh. Chem.* **2017**, *148*, 1069−1074.
(98) The Synthesis of Molybdenum and Tungsten Dinitrogen Complexes. In *Inorganic Syntheses*; Wiley: 1980; pp 119−127.
(99) Cotton, F. A.; Zingales, F. Donor-Acceptor Properties of Isonitriles as Estimated by Infrared Study. *J. Am. Chem. Soc.* **1961**, *83*, 351−355.
(100) Hahn, F. E. The Coordination Chemistry of Multidentate Isocyanide Ligands. *Angew. Chem., Int. Ed. Engl.* **1993**, *32*, 650−665.
(101) Margulieux, G. W.; Weidemann, N.; Lacy, D. C.; Moore, C. E.; Rheingold, A. L.; Figueroa, J. S. Isocyano Analogues of $Co(CO)_4^n$: A Tetraisocyanide of Cobalt Isolated in Three States of Charge. *J. Am. Chem. Soc.* **2010**, *132*, 5033−5035.
(102) Drance, M. J.; Sears, J. D.; Mrse, A. M.; Moore, C. E.; Rheingold, A. L.; Neidig, M. L.; Figueroa, J. S. Terminal coordination of diatomic boron monofluoride to iron. *Science* **2019**, *363*, 1203−1205.
(103) Kvapilova, H.; Sattler, W.; Sattler, A.; Sazanovich, I. V.; Clark, I. P.; Towrie, M.; Gray, H. B.; Zalis, S.; Vlcek, A. Electronic excited states of tungsten(0) arylisocyanides. *Inorg. Chem.* **2015**, *54*, 8518−8528.
(104) Wei, Y.; Zheng, M.; Chen, L.; Zhou, X.; Liu, S. Near-infrared to violet triplet−triplet annihilation fluorescence upconversion of Os(II) complexes by strong spin-forbidden transition. *Dalton Trans.* **2019**, *48*, 11763−11771.

https://dx.doi.org/10.1021/jacs.0c12805
J. Am. Chem. Soc. 2021, 143, 1651−1663

(105) Caspar, J. V.; Kober, E. M.; Sullivan, B. P.; Meyer, T. J. Application of the energy gap law to the decay of charge-transfer excited states. *J. Am. Chem. Soc.* **1982**, *104*, 630−632.
(106) Kober, E. M.; Sullivan, B. P.; Dressick, W. J.; Caspar, J. V.; Meyer, T. J. Highly Luminescent Polypyridyl Complexes of Osmium(II). *J. Am. Chem. Soc.* **1980**, *102*, 7383−7385.
(107) Caspar, J. V.; Meyer, T. J. Photochemistry of $Ru(bpy)_3^{2+}$ - Solvent effects. *J. Am. Chem. Soc.* **1983**, *105*, 5583−5590.
(108) Soupart, A.; Alary, F.; Heully, J. L.; Elliott, P. I. P.; Dixon, I. M. Recent progress in ligand photorelease reaction mechanisms: Theoretical insights focusing on Ru(II) ^{3}MC states. *Coord. Chem. Rev.* **2020**, *408*, 213184.
(109) Sun, Q. C.; Dereka, B.; Vauthey, E.; Daku, L. M. L.; Hauser, A. Ultrafast transient IR spectroscopy and DFT calculations of ruthenium(II) polypyridyl complexes. *Chem. Sci.* **2017**, *8*, 223−230.
(110) Hager, G. D.; Crosby, G. A. Charge-transfer exited states of ruthenium(II) complexes. I. Quantum yield and decay measurements. *J. Am. Chem. Soc.* **1975**, *97*, 7031−7037.
(111) Van Houten, J.; Watts, R. J. Temperature-Dependence of Photophysical and Photochemical Properties of Tris(2,2′-bipyridyl)-ruthenium(II) Ion in Aqueous-Solution. *J. Am. Chem. Soc.* **1976**, *98*, 4853−4858.
(112) Damrauer, N. H.; Boussie, T. R.; Devenney, M.; McCusker, J. K. Effects of Intraligand Electron Delocalization, Steric Tuning, and Excited-State Vibronic Coupling on the Photophysics of Aryl-Substituted Bipyridyl Complexes of Ru(II). *J. Am. Chem. Soc.* **1997**, *119*, 8253−8268.
(113) Müller, P.; Brettel, K. $[Ru(bpy)_3]^{2+}$ as a reference in transient absorption spectroscopy: differential absorption coefficients for formation of the long-lived ^{3}MLCT excited state. *Photochem. Photobiol. Sci.* **2012**, *11*, 632−636.
(114) Montalti, M.; Credi, A.; Prodi, L.; Gandolfi, M. T. *Handbook of Photochemistry*; CRC Taylor & Francis: Boca Raton, FL, 2006.
(115) Pedersen, S. U.; Christensen, T. B.; Thomasen, T.; Daasbjerg, K. New methods for the accurate determination of extinction and diffusion coefficients of aromatic and heteroaromatic radical anions in N,N-dimethylformamide. *J. Electroanal. Chem.* **1998**, *454*, 123−143.
(116) Murtaza, Z.; Graff, D. K.; Zipp, A. P.; Worl, L. A.; Jones, W. E., Jr.; Bates, W. D.; Meyer, T. J. Energy Transfer in the Inverted Region: Calculation of Relative Rate Constants by Emission Spectral Fitting. *J. Phys. Chem.* **1994**, *98*, 10504−10513.
(117) Singh-Rachford, T. N.; Castellano, F. N. Photon upconversion based on sensitized triplet-triplet annihilation. *Coord. Chem. Rev.* **2010**, *254*, 2560−2573.
(118) Haruki, R.; Sasaki, Y.; Masutani, K.; Yanai, N.; Kimizuka, N. Leaping across the visible range: near-infrared-to-violet photon upconversion employing a silyl-substituted anthracene. *Chem. Commun.* **2020**, *56*, 7017−7020.
(119) Nishimura, N.; Gray, V.; Allardice, J. R.; Zhang, Z.; Pershin, A.; Beljonne, D.; Rao, A. Photon Upconversion from Near-Infrared to Blue Light with TIPS-Anthracene as an Efficient Triplet−Triplet Annihilator. *ACS Mater. Lett.* **2019**, *1*, 660−664.
(120) Kiseleva, N.; Nazari, P.; Dee, C.; Busko, D.; Richards, B. S.; Seitz, M.; Howard, I. A.; Turshatov, A. Lanthanide Sensitizers for Large Anti-Stokes Shift Near-Infrared-to-Visible Triplet-Triplet Annihilation Photon Upconversion. *J. Phys. Chem. Lett.* **2020**, *11*, 2477−2481.
(121) Haefele, A.; Blumhoff, J.; Khnayzer, R. S.; Castellano, F. N. Getting to the (Square) Root of the Problem: How to Make Noncoherent Pumped Upconversion Linear. *J. Phys. Chem. Lett.* **2012**, *3*, 299−303.
(122) Zhou, Y.; Castellano, F. N.; Schmidt, T. W.; Hanson, K. On the Quantum Yield of Photon Upconversion via Triplet−Triplet Annihilation. *ACS Energy Lett.* **2020**, *5*, 2322−2326.
(123) López-Calixto, C. G.; Liras, M.; de la Peña O'Shea, V. A.; Pérez-Ruiz, R. Synchronized biphotonic process triggering CC coupling catalytic reactions. *Appl. Catal., B* **2018**, *237*, 18−23.
(124) Kerzig, C.; Wenger, O. S. Sensitized triplet−triplet annihilation upconversion in water and its application to photochemical transformations. *Chem. Sci.* **2018**, *9*, 6670−6678.
(125) Islangulov, R. R.; Castellano, F. N. Photochemical upconversion: Anthracene dimerization sensitized to visible light by a Ru-II chromophore. *Angew. Chem., Int. Ed.* **2006**, *45*, 5957−5959.
(126) Kalyanasundaram, K. Photophysics, photochemistry and solar energy conversion with tris(bipyridyl)ruthenium(II) and its analogues. *Coord. Chem. Rev.* **1982**, *46*, 159−244.
(127) Wrighton, M.; Markham, J. Quenching of the luminescent state of tris(2,2′-bipyridine)ruthenium(II) by electronic energy transfer. *J. Phys. Chem.* **1973**, *77*, 3042−3044.
(128) Börjesson, K.; Dzebo, D.; Albinsson, B.; Moth-Poulsen, K. Photon upconversion facilitated molecular solar energy storage. *J. Mater. Chem. A* **2013**, *1*, 8521−8524.
(129) Askes, S. H. C.; Kloz, M.; Bruylants, G.; Kennis, J. T. M.; Bonnet, S. Triplet−triplet annihilation upconversion followed by FRET for the red light activation of a photodissociative ruthenium complex in liposomes. *Phys. Chem. Chem. Phys.* **2015**, *17*, 27380−27390.
(130) Askes, S. H. C.; Bahreman, A.; Bonnet, S. Activation of a Photodissociative Ruthenium Complex by Triplet-Triplet Annihilation Upconversion in Liposomes. *Angew. Chem., Int. Ed.* **2014**, *53*, 1029−1033.
(131) Khnayzer, R. S.; Blumhoff, J.; Harrington, J. A.; Haefele, A.; Deng, F.; Castellano, F. N. Upconversion-powered photoelectrochemistry. *Chem. Commun.* **2012**, *48*, 209−211.
(132) Kwon, O. S.; Kim, J.-H.; Cho, J. K.; Kim, J.-H. Triplet−Triplet Annihilation Upconversion in CdS-Decorated SiO_2 Nanocapsules for Sub-Bandgap Photocatalysis. *ACS Appl. Mater. Interfaces* **2015**, *7*, 318−325.
(133) Jiang, Z.; Xu, M.; Li, F.; Yu, Y. Red-Light-Controllable Liquid-Crystal Soft Actuators via Low-Power Excited Upconversion Based on Triplet−Triplet Annihilation. *J. Am. Chem. Soc.* **2013**, *135*, 16446−16453.
(134) Blum, T. R.; Miller, Z. D.; Bates, D. M.; Guzei, I. A.; Yoon, T. P. Enantioselective Photochemistry Through Lewis Acid-Catalyzed Triplet Energy Transfer. *Science* **2016**, *354*, 1391−1395.
(135) Molloy, J. J.; Schäfer, M.; Wienhold, M.; Morack, T.; Daniliuc, C. G.; Gilmour, R. Boron-enabled geometric isomerization of alkenes via selective energy-transfer catalysis. *Science* **2020**, *369*, 302−306.
(136) Holzl-Hobmeier, A.; Bauer, A.; Silva, A. V.; Huber, S. M.; Bannwarth, C.; Bach, T. Catalytic deracemization of chiral allenes by sensitized excitation with visible light. *Nature* **2018**, *564*, 240−243.
(137) Teders, M.; Henkel, C.; Anhauser, L.; Strieth-Kalthoff, F.; Gomez-Suarez, A.; Kleinmans, R.; Kahnt, A.; Rentmeister, A.; Guldi, D.; Glorius, F. The energy-transfer-enabled biocompatible disulfide-ene reaction. *Nat. Chem.* **2018**, *10*, 981−988.
(138) Becker, M. R.; Wearing, E. R.; Schindler, C. S. Synthesis of azetidines via visible-light-mediated intermolecular [2 + 2] photocycloadditions. *Nat. Chem.* **2020**, *12*, 898−905.
(139) Zhou, Q.-Q.; Zou, Y.-Q.; Lu, L.-Q.; Xiao, W.-J. Visible-Light-Induced Organic Photochemical Reactions through Energy-Transfer Pathways. *Angew. Chem., Int. Ed.* **2019**, *58*, 1586−1604.
(140) Xu, B.; Troian-Gautier, L.; Dykstra, R.; Martin, R. T.; Gutierrez, O.; Tambar, U. K. Photocatalyzed Diastereoselective Isomerization of Cinnamyl Chlorides to Cyclopropanes. *J. Am. Chem. Soc.* **2020**, *142*, 6206−6215.
(141) Tian, L.; Till, N. A.; Kudisch, B.; MacMillan, D. W. C.; Scholes, G. D. Transient Absorption Spectroscopy Offers Mechanistic Insights for an Iridium/Nickel-Catalyzed C-O Coupling. *J. Am. Chem. Soc.* **2020**, *142*, 4555−4559.
(142) Lu, J.; Pattengale, B.; Liu, Q.; Yang, S.; Shi, W.; Li, S.; Huang, J.; Zhang, J. Donor−Acceptor Fluorophores for Energy-Transfer-Mediated Photocatalysis. *J. Am. Chem. Soc.* **2018**, *140*, 13719−13725.
(143) Paulus, B. C.; Adelman, S. L.; Jamula, L. L.; McCusker, J. K. Leveraging excited-state coherence for synthetic control of ultrafast dynamics. *Nature* **2020**, *582*, 214−218.

https://dx.doi.org/10.1021/jacs.0c12805
J. Am. Chem. Soc. 2021, 143, 1651−1663